
Supplementary information

Adaptive adversarial neural networks for the analysis of lossy and domain-shifted datasets of medical images

In the format provided by the authors and unedited

Nomenclature:

	D	[S – Sperm, E – Embryo, M – Malaria/Redblood cells]
DYst	Y	[M – Model, D – Dataset]
	s	[data distribution]
	t	[data distribution]

For dataset and imaging system nomenclature, s is graded from 4 through 1, with 4 being the dataset/imaging system of highest quality image (clinical microscope systems) and 1 being the dataset/imaging system of lowest quality (smartphone microscope systems). For example, ED4 denotes the embryo dataset imaged using a clinical Embryoscope that was used by embryologists for the annotations.

t is only used when defining domain adaption models, to denote source (s) and target (t) that were used when developing the model. For example, EM41 denotes a model (M) trained on embryo datasets (E) with Embryoscope images (4) as its source and smartphone images (1) as its target.

Network development hardware and software

MD-nets were implemented with Python 3.6 using PyTorch (v1.5.0). Other publicly available libraries used include OS, time, csv, sklearn, math, copy, Itertools, random, and NumPy. The network was developed using a computer running Linux Ubuntu 18.04. The network training was GPU-bound, and the training was performed using 3 GeForce GTX 1080Ti GPUs (Nvidia). Some networks were also trained using V100 (Nvidia) clusters.

Template matching

Template Matching was used to extract individual cells from sample slide images. A sliding window approach was used to compare the template image of a single cell with the images of the slides. The Normalised Correlation metric was used to evaluate the similarity between the template and the regions within the slide images. Then, non-Max Suppression was applied to remove redundant detections of the same region. Intersection over Union was used to calculate the overlapping area of the detected patches. If the normalised overlapping area exceeded the overlap threshold, the detection was discarded. Among all the overlapping patches, the one with the best match threshold was considered. The algorithm made sure to identify the rotated and scaled occurrences. For MD1 images, a match threshold of 0.7, an overlap threshold of 0.9, and a template size of 250 x 250 were used. For MD2 images, a match threshold of 0.6, an overlap threshold of 0.9, and a template size of 220 x 220 were used. For MD3 images, a match threshold of 0.6, an overlap threshold of 0.9, and a template size of 100 x 100 were used. For SD1 images, a match threshold of 0.8, an overlap threshold of 0.7, and a template size of $\sim(146 \times 146)$ were used. For SD2 images, a match threshold of 0.5, an overlap threshold of 0.8, and a template size of 280 x 280 were used. For SD3 images, a match threshold of 0.8, an overlap threshold of 0.8, and a template size of 60 x 60 were used. For SD4 images, a match threshold of 0.8, an overlap threshold of 0.8, and a template size of 130 x 130 were used. The algorithm was implemented using the OpenCV and Multi-Template-Matching libraries.

Receiver Operating Characteristic analysis

The Receiver Operating Characteristic (ROC) curve was plotted between the sensitivity and specificity for various confidence thresholds. The Area Under the ROC is used to measure the

performance of a classification model by measuring its degree of separability. The Scikit-learn library was used to plot the ROC curves and calculate the area under the curve.

t-SNE

t-SNE (t-Distributed Stochastic Neighbor Embedding) is an unsupervised, non-linear dimensionality reduction technique to visualise high dimensional data. This technique was used to visualise the source and target distributions and track the results of domain adaption. We used perplexity values in the range of [0,50]. The relative position of the target and source feature space was examined to see if the adversarial network was successful in adapting the target domain to the source domain. The separation of classes within each domain was also compared to see the ability of the network in the classification of unlabelled target data after being trained with the labelled source dataset.

Saliency maps

Saliency maps were used to examine if the network utilized features that were potentially relevant to make classification decisions. Class-specific gradient information flowing into the final convolutional layer of the network was used to produce a localisation map of the important regions within the image, and to verify if the saliency output coincided with the actual discriminative region of the image. A PyTorch implementation of Gradient-weighted Class Activation Mapping was used to visualise the final feature map of the classifier in the trained adversarial network.

Commercial Benchtop microscope system for sperm and malaria imaging (SD3 and MD3)

SD3 and MD3 datasets were obtained using a benchtop microscope (Microscope BZ-X800, KEYENCE) equipped with a 60×/0.85NA objective lens (Nikon CFI Plan Fluor 60XC) under

bright field illumination. The resolution of the resultant system was estimated to be $<0.78 \mu\text{m}$ ($>912 \text{ lp/mm}$) using a USAF 1951 resolution target (Fig. S11).

Portable standalone optical system for imaging human embryos (ED2)

A portable stand-alone imaging system that consists of a single-board computer (Raspberry Pi 3B+), an LED (Microtivity, IL041), a complementary metal-oxide-semiconductor (CMOS) sensor, and an objective lens was developed. The enclosure for the system was designed in SolidWorks and 3-D printed using an Ultimaker 2 Extended with Ultimaker PLA (polylactic acid) as the printing material. The embryo cells were first magnified using a 10X Plan Achromatic Objective Lens (Amscope PA10X-B) and illuminated by a battery-powered LED. The magnified image of the cells was captured by the CMOS sensor which was placed in line with the objective lens. The CMOS sensor was connected to a single-board computer (SBC) which retrieved the image from the CMOS sensor. The SBC then transferred the recorded embryo images to a smartphone through the Bluetooth module for analysis. The resolution of the resultant system was estimated to be $4.38 \mu\text{m}$ ($\sim 114 \text{ lp/mm}$) using a USAF 1951 resolution target (Fig. S11).

Portable optical system for imaging sperm and blood cells (SD2 and MD2)

For imaging sperm and blood cells, a portable optical system was constructed using 3D-printed parts, a single board computer, a CMOS camera, and an achromatic lens. The device enclosure was designed using SolidWorks (Dassault Systems) and 3D-printed with an Ultimaker 2+ Extended 3D-printer using Polylactic acid (PLA) as printing material. The system comprises mechanical, optical, and electrical units that function together to image the sample.

The mechanical part of the optical system is responsible for enabling the sample holder's motion along the X-axis and Z-axis. A T8 trapezoidal thread precision lead screw attached to a NEMA 17 Stepper Motor (Part No.: AW0004 from Iverntech) was used with a nut attached to the slide holder

base to provide linear motion along the Z-axis. Support to the Z-axis motion was obtained using 6 mm linear guide rods with LM6UU bearings for precise motion. The minimum step possible in the Z-direction was about 2.5 μ m. An M3 lead screw attached to a 30 RPM 6V DC motor was used with an M3 nut attached to the slide holder to provide motion along with the X-axis. The lead screw of the DC motor was used with 3 mm guide rods to support the slide holder in order to facilitate stable movement along the X-direction. The minimum step possible in the X-direction was 50 microns. This system can image a 30 mm linear channel within the slide which counts for around 300 images per slide.

The optical unit of the portable standalone device consists of a high magnification 60X Plain Achromatic Objective Lens (Amscope PA60XK-V300) to magnify the sample placed in the slide holder. An 8-MP CMOS Pi-Camera V2 was used to capture the magnified sample. The objective lens and CMOS camera were placed 60mm apart for target magnification. A 10 W white COB LED chip was used to illuminate the slide. The focus of the image was adjusted by energising the stepper motor, thereby adjusting the position of the sample holder base.

The electrical unit of the standalone system primarily consists of circuits that interface the NEMA 17 MI polar stepper motor and the 6 V DC motor to the single board computer using the A4988 stepper driver and dual H-bridge L298N driver, respectively. The A4988 stepper driver was set to 1/32 micro-stepping mode to achieve a step of 2.5 μ m along the Z-axis. The DC motor was actuated in intervals of 100 microseconds to achieve a step of 50 μ m along the X-axis using the ON-OFF control. The motor drivers were powered by a 12V 2.0A adapter connected to the main supply. The resolution of the resultant system was estimated to be 0.98 μ m (~512 lp/mm) using a USAF 1951 resolution target (Fig. S11).

Smartphone-based optical system for imaging human embryos (ED1)

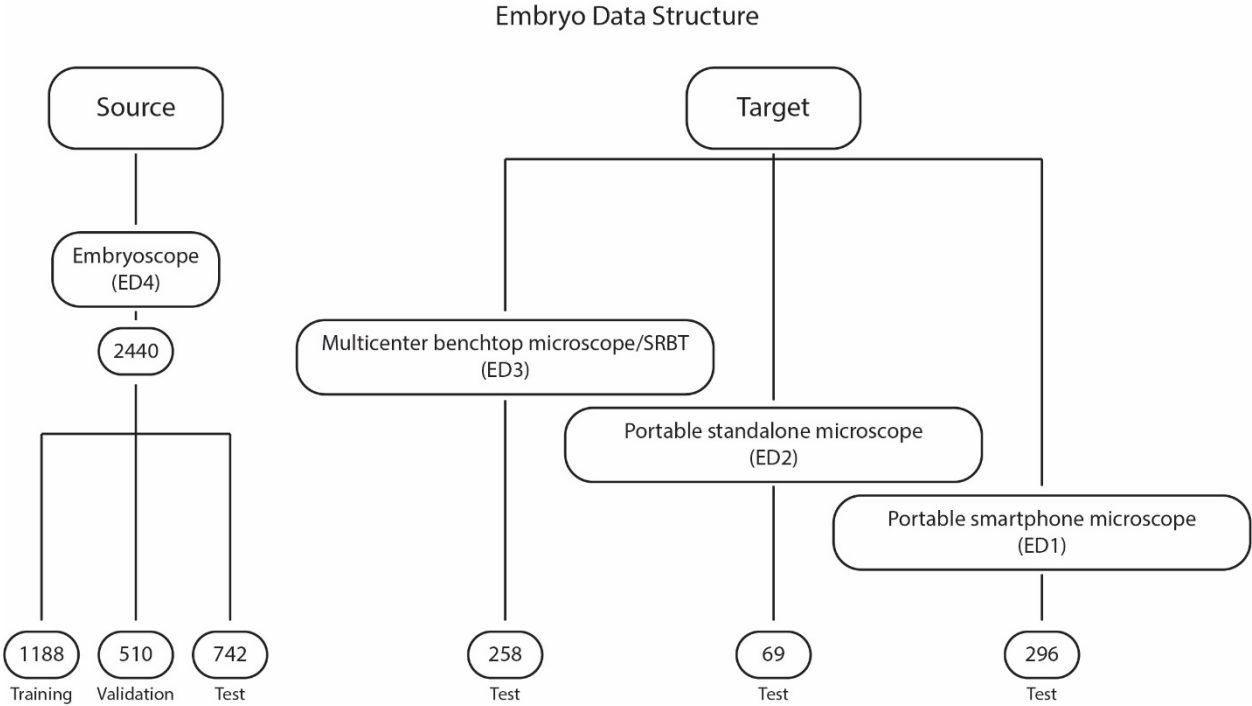
An optical attachment for smartphones that houses a plano-convex lens obtained from the pick-up heads of a DVD drive, a coin battery (Panasonic, CR1620), and an LED (Microtivity, IL041) was developed. The smartphone attachment was particularly designed for a Moto X smartphone (Motorola, XT1575) in Solid Works and 3D-printed using an Ultimaker 2 Extended with Ultimaker PLA (polylactic acid) as the printing material. The plano-convex lens was positioned inside the optical attachment such that it was aligned with the optical axis of the smartphone's front camera. Embryos were illuminated by the battery-powered LED. Sample fine focus was achieved through the smartphone's autofocus capability. The resolution of the resultant system was estimated to be $3.1 \mu\text{m}$ ($\sim 161 \text{ lp/mm}$) using a USAF 1951 resolution target (Fig. S11).

Smartphone-based optical system for imaging sperm cells (SD1)

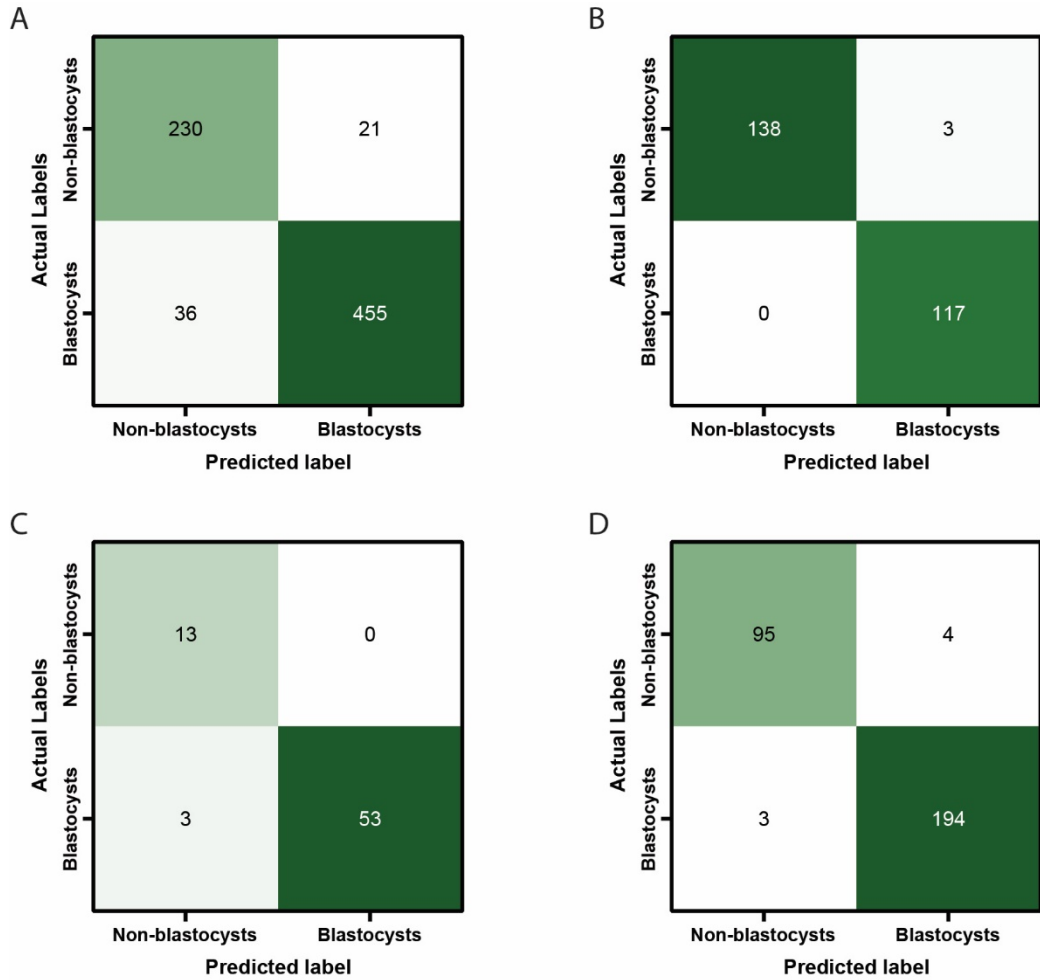
The smartphone-based optical system developed for sperm imaging houses a pair of lenses obtained from the pick-up heads of a DVD and CD drive, a coin battery (Panasonic, CR1620), and an LED (Microtivity, IL041). The enclosure was 3D-printed using an Ultimaker 2 Extended with Ultimaker PLA (polylactic acid) as the printing material. The lenses were positioned inside the optical smartphone attachment such that they were aligned with the optical axis of the smartphone's rear camera. The 3D model of the attachment was designed in SolidWorks for a Moto X smartphone (Motorola, XT1575). The sperm cells were illuminated by a LED. Sample fine focus was achieved through the smartphone's autofocus capability. The resolution of the resultant system was estimated to be $1.74 \mu\text{m}$ ($\sim 287 \text{ lp/mm}$) using a USAF 1951 resolution target (Fig. S11).

Smartphone optical system for imaging blood cells (MD1)

MD1 dataset was obtained using a setup that consisted of a smartphone that was attached to a compound microscope. The rear camera of the smartphone was positioned such that it was aligned with the optical axis of the eyepiece of the compound microscope (OMAX, M828D50-CA). The MD1 images were captured using a 40/0.85 Plan Objective lens of the microscope under bright-field illumination. The resolution of the resultant system was estimated to be $<0.78 \mu\text{m}$ ($>912 \text{ lp/mm}$) using a USAF 1951 resolution target (Fig. S11).

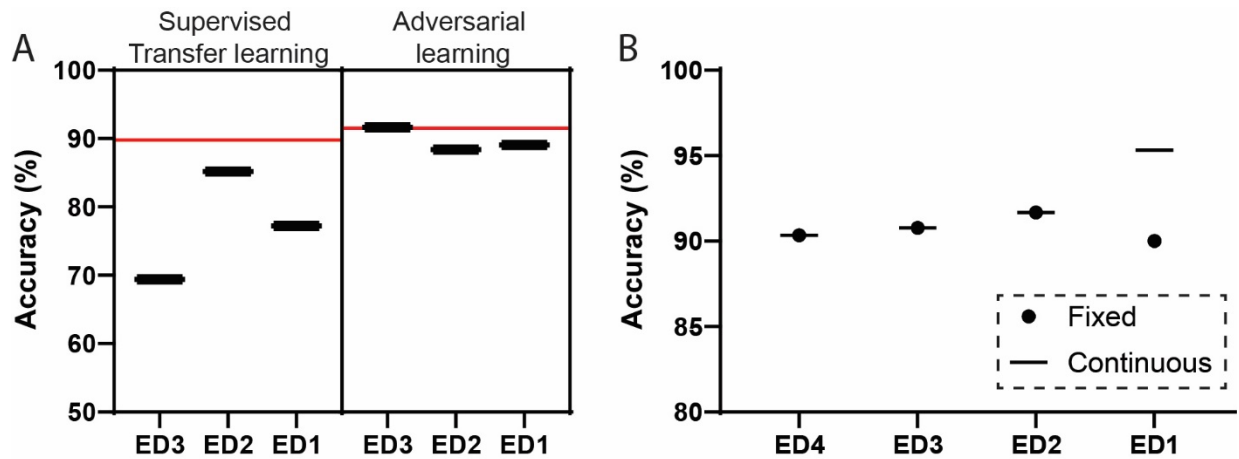


Supplementary Figure 1 | Data structure of embryo images utilised in the development and evaluation of the neural networks. All embryo images were annotated by expert embryology staff.

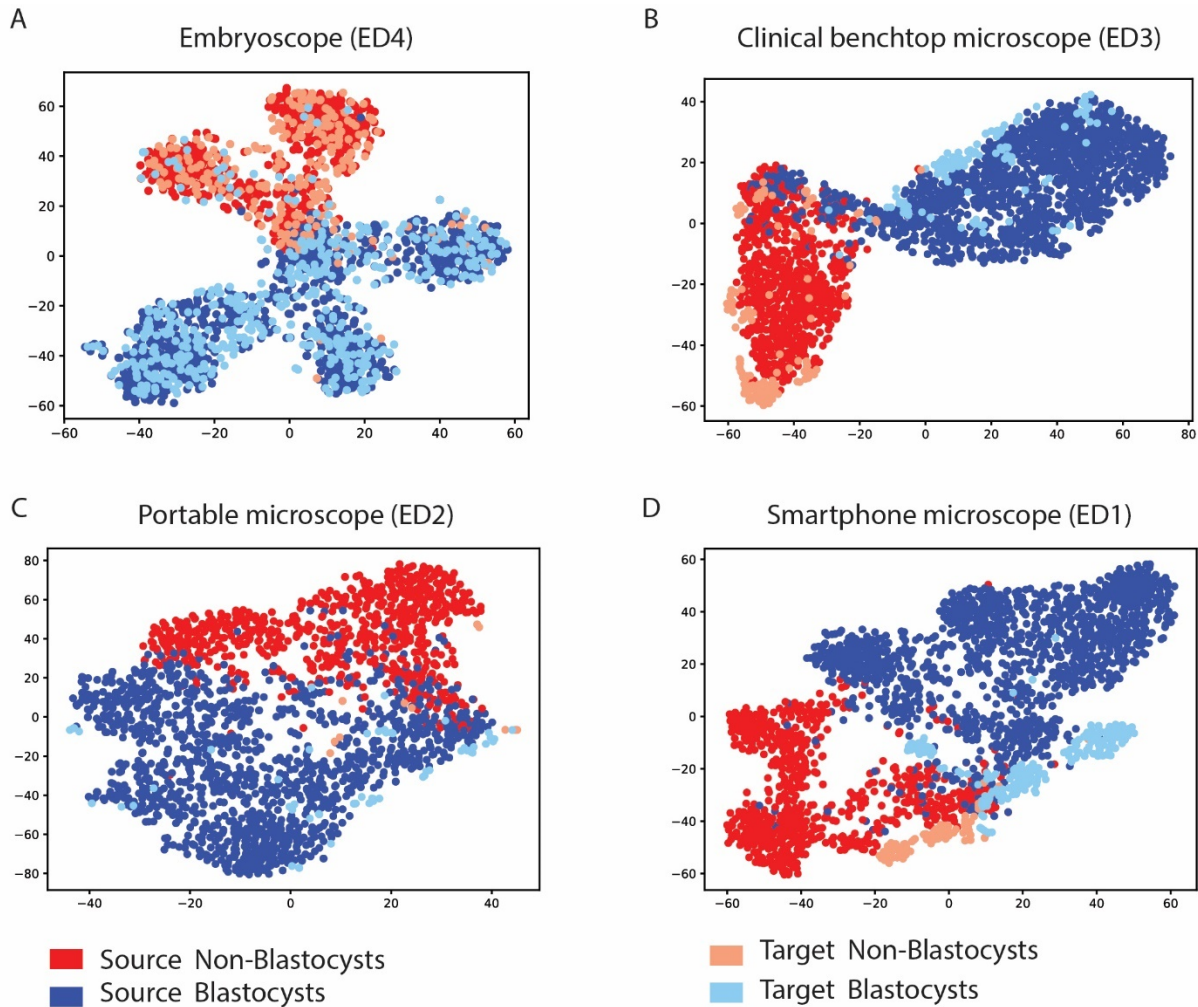


Supplementary Figure 2 | Confusion matrices of MD-nets in the evaluation of embryo images. (A) Confusion matrix of MD-net in differentiating between blastocysts and non-blastocysts by evaluating embryo images collected using an Embryoscope (ED4, n=742). (B) Confusion matrix of MD-net in differentiating between blastocysts and non-blastocysts by evaluating embryo images collected using various benchtop microscopes at different fertility centers around the country (ED3, n=258). (C) Confusion matrix of MD-net in differentiating between blastocysts and non-blastocysts by evaluating embryo images collected using a portable 3D-printed microscope (ED2, n=69). (D) Confusion matrix of MD-net in differentiating between

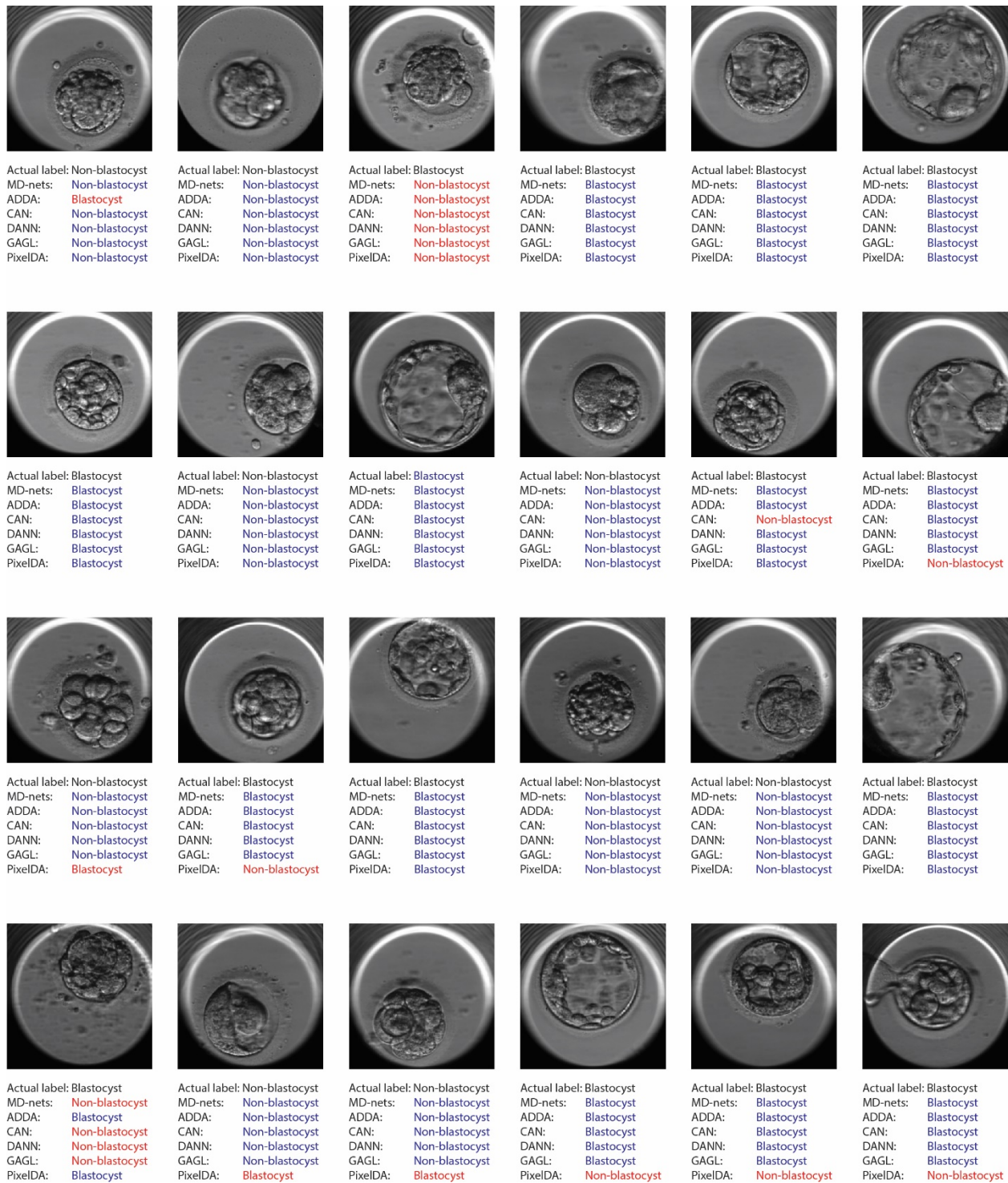
blastocysts and non-blastocysts by evaluating embryo images collected using a smartphone-based portable microscope (ED1, n=296).



Supplementary Figure 3 | MD-nets evaluations using embryo images. (A) Comparison of performance on source data after adaption through supervised transfer learning and MD-nets (n=742). The red line indicates the baseline performance of the supervised Xception and MD-net (Xception) models trained using the source (ED4) training dataset, on the source (ED4) test data. The black lines indicate the performance of models trained through transfer learning and MD-nets using ED3, ED2, and ED1 as the target dataset, on ED4 test data. (B) Comparison of performances when MD-net weights are fixed after adaption and when weights are allowed to update with unseen unlabelled data.

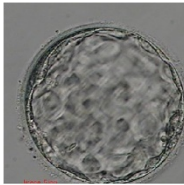
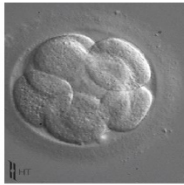

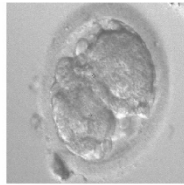





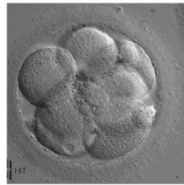

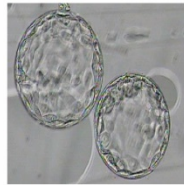

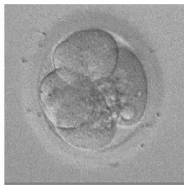






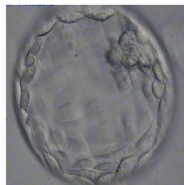

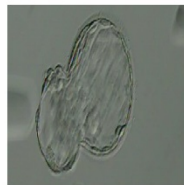



Supplementary Figure 4 | t-SNE plots of MD-nets representing both source and target in the evaluation of embryo images. (A) t-SNE plot showing the distribution of source (ED4) and target (ED4) embryo images. (B) t-SNE plot showing the distribution of source (ED4) and target (ED3) embryo images. (C) t-SNE plot showing the distribution of source (ED4) and target (ED2) embryo images. (D) t-SNE plot showing the distribution of source (ED4) and target (ED1) embryo images. Dark red and dark blue dots represent embryo images belonging to the source non-blastocyst and blastocyst classes, respectively. Light red and light blue dots represent embryo images belonging to the target non-blastocyst and blastocyst classes, respectively.



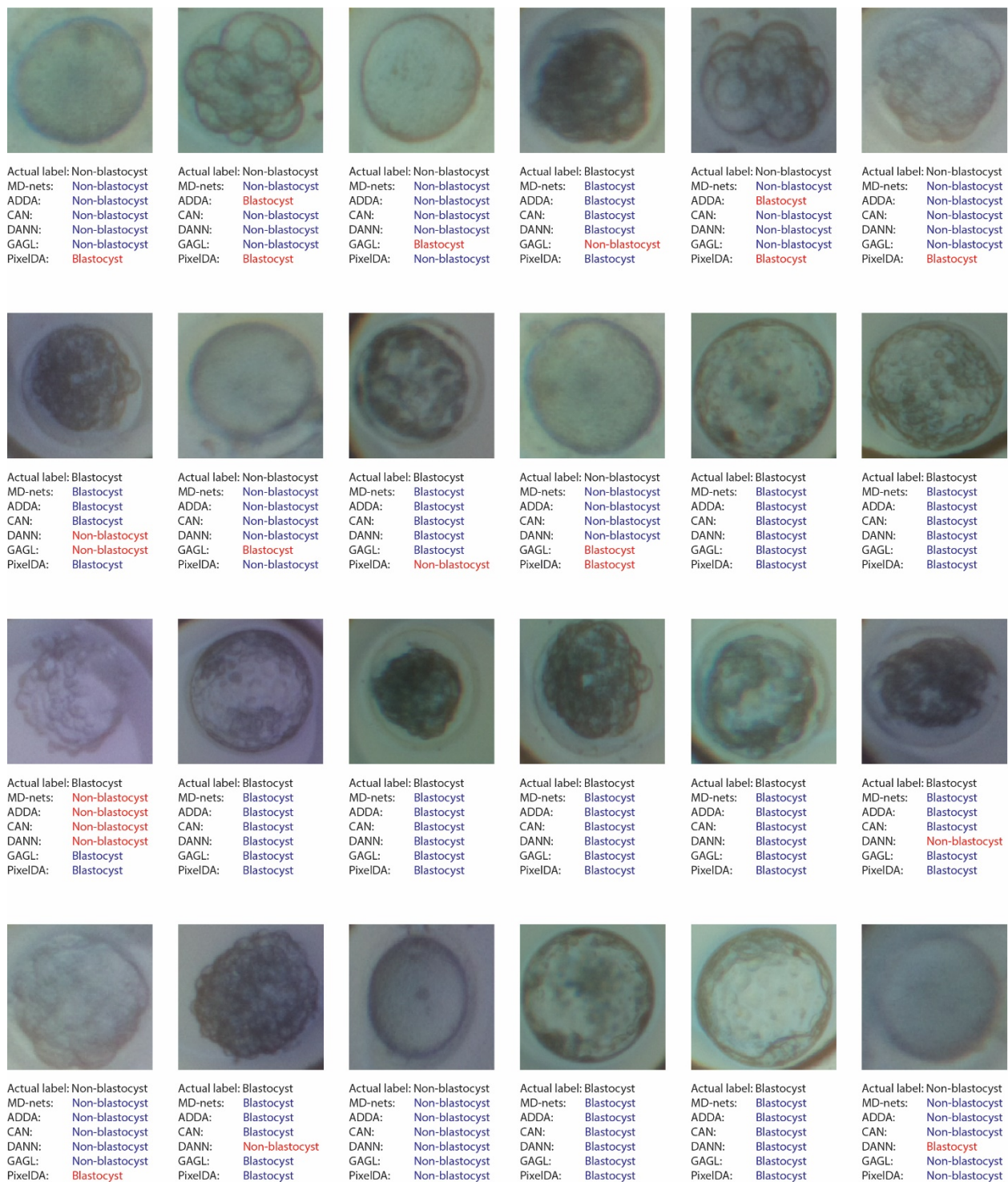
Supplementary Figure 5 | Sampled images from the embryo dataset (ED4) as evaluated by different domain adaption approaches. The networks were trained to classify between the blastocyst and non-blastocyst embryo images using labelled and unlabelled ED4 training data and

the best performing models were used in evaluating the sampled images. The images were sampled from the ED4 test dataset such that the results across these images matched closely with the overall results of each method, so as to be best indicative of the performance differences between models.

					
Actual label: Blastocyst MD-nets: Blastocyst ADDA: Blastocyst CAN: Blastocyst DANN: Blastocyst GAGL: Blastocyst PixelDA: Non-blastocyst	Actual label: Non-blastocyst MD-nets: Non-blastocyst ADDA: Non-blastocyst CAN: Non-blastocyst DANN: Non-blastocyst GAGL: Non-blastocyst PixelDA: Non-blastocyst	Actual label: Non-blastocyst MD-nets: Non-blastocyst ADDA: Non-blastocyst CAN: Non-blastocyst DANN: Non-blastocyst GAGL: Non-blastocyst PixelDA: Non-blastocyst	Actual label: Non-blastocyst MD-nets: Non-blastocyst ADDA: Non-blastocyst CAN: Non-blastocyst DANN: Non-blastocyst GAGL: Non-blastocyst PixelDA: Non-blastocyst	Actual label: Blastocyst MD-nets: Blastocyst ADDA: Blastocyst CAN: Blastocyst DANN: Blastocyst GAGL: Blastocyst PixelDA: Blastocyst	Actual label: Blastocyst MD-nets: Blastocyst ADDA: Blastocyst CAN: Blastocyst DANN: Blastocyst GAGL: Non-blastocyst PixelDA: Blastocyst
					
Actual label: Blastocyst MD-nets: Blastocyst ADDA: Blastocyst CAN: Blastocyst DANN: Blastocyst GAGL: Blastocyst PixelDA: Blastocyst	Actual label: Non-blastocyst MD-nets: Non-blastocyst ADDA: Non-blastocyst CAN: Non-blastocyst DANN: Blastocyst GAGL: Non-blastocyst PixelDA: Non-blastocyst	Actual label: Non-blastocyst MD-nets: Non-blastocyst ADDA: Non-blastocyst CAN: Non-blastocyst DANN: Non-blastocyst GAGL: Non-blastocyst PixelDA: Non-blastocyst	Actual label: Non-blastocyst MD-nets: Non-blastocyst ADDA: Non-blastocyst CAN: Non-blastocyst DANN: Non-blastocyst GAGL: Blastocyst PixelDA: Non-blastocyst	Actual label: Blastocyst MD-nets: Blastocyst ADDA: Blastocyst CAN: Blastocyst DANN: Blastocyst GAGL: Non-blastocyst PixelDA: Blastocyst	Actual label: Blastocyst MD-nets: Blastocyst ADDA: Blastocyst CAN: Blastocyst DANN: Blastocyst GAGL: Blastocyst PixelDA: Blastocyst
					
Actual label: Blastocyst MD-nets: Blastocyst ADDA: Blastocyst CAN: Blastocyst DANN: Blastocyst GAGL: Blastocyst PixelDA: Blastocyst	Actual label: Non-blastocyst MD-nets: Non-blastocyst ADDA: Non-blastocyst CAN: Non-blastocyst DANN: Non-blastocyst GAGL: Non-blastocyst PixelDA: Non-blastocyst	Actual label: Non-blastocyst MD-nets: Non-blastocyst ADDA: Non-blastocyst CAN: Non-blastocyst DANN: Non-blastocyst GAGL: Non-blastocyst PixelDA: Non-blastocyst	Actual label: Blastocyst MD-nets: Blastocyst ADDA: Blastocyst CAN: Blastocyst DANN: Blastocyst GAGL: Blastocyst PixelDA: Non-blastocyst	Actual label: Non-blastocyst MD-nets: Non-blastocyst ADDA: Non-blastocyst CAN: Non-blastocyst DANN: Non-blastocyst GAGL: Non-blastocyst PixelDA: Non-blastocyst	Actual label: Non-blastocyst MD-nets: Non-blastocyst ADDA: Non-blastocyst CAN: Non-blastocyst DANN: Non-blastocyst GAGL: Non-blastocyst PixelDA: Non-blastocyst
					
Actual label: Blastocyst MD-nets: Blastocyst ADDA: Blastocyst CAN: Blastocyst DANN: Blastocyst GAGL: Blastocyst PixelDA: Blastocyst	Actual label: Blastocyst MD-nets: Blastocyst ADDA: Blastocyst CAN: Blastocyst DANN: Blastocyst GAGL: Blastocyst PixelDA: Blastocyst	Actual label: Blastocyst MD-nets: Blastocyst ADDA: Blastocyst CAN: Blastocyst DANN: Blastocyst GAGL: Blastocyst PixelDA: Non-blastocyst	Actual label: Non-blastocyst MD-nets: Non-blastocyst ADDA: Non-blastocyst CAN: Non-blastocyst DANN: Non-blastocyst GAGL: Non-blastocyst PixelDA: Non-blastocyst	Actual label: Blastocyst MD-nets: Blastocyst ADDA: Non-blastocyst CAN: Blastocyst DANN: Blastocyst GAGL: Blastocyst PixelDA: Blastocyst	Actual label: Non-blastocyst MD-nets: Non-blastocyst ADDA: Non-blastocyst CAN: Non-blastocyst DANN: Non-blastocyst GAGL: Non-blastocyst PixelDA: Non-blastocyst

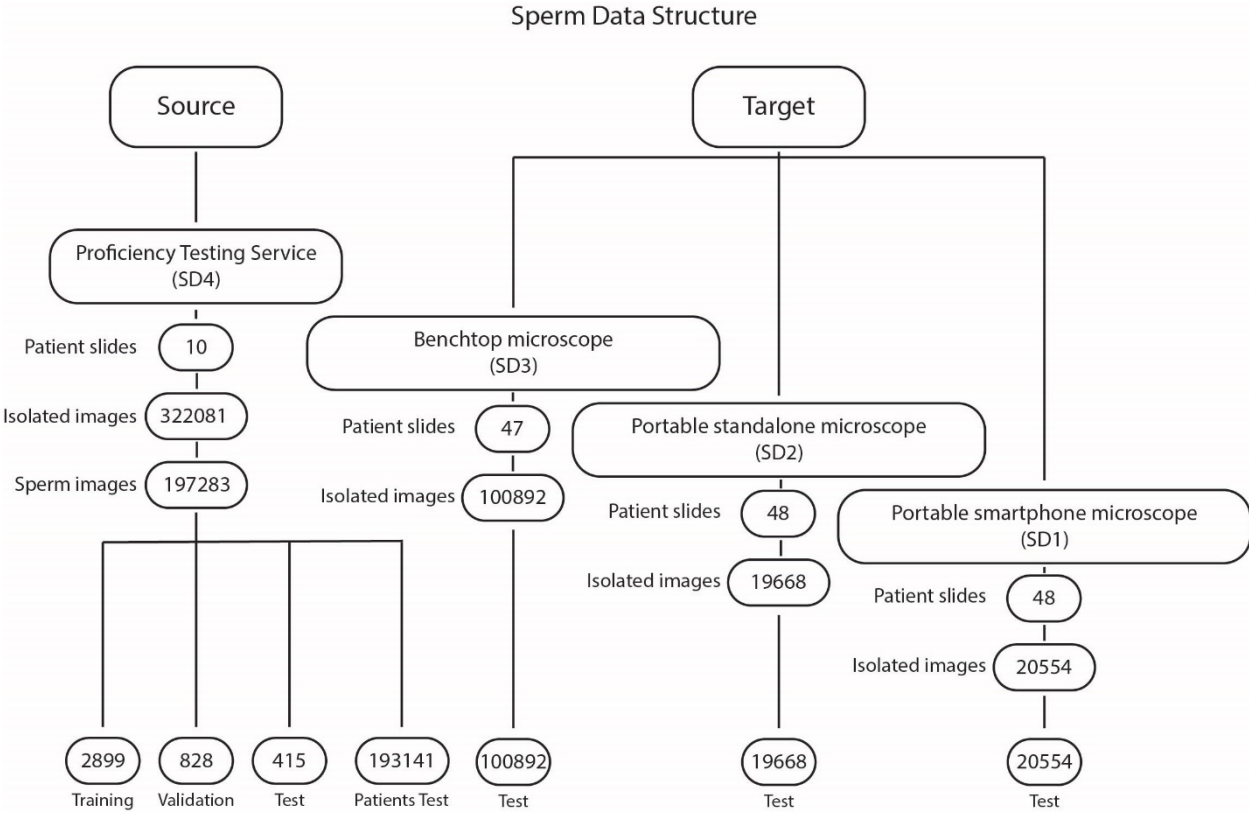
Supplementary Figure 6 | Sampled images from the embryo dataset (ED3) as evaluated by different domain adaption approaches. The networks were trained to classify between the blastocyst and non-blastocyst embryo images using labelled ED4 and unlabelled ED3 training data and the best performing models were used in evaluating the sampled images. The images were sampled from ED3 test dataset such that the results across these images matched closely with the overall results of each method, so as to be best indicative of the performance differences between models.

and the best performing models were used in evaluating the sampled images. The images were sampled from ED2 test dataset such that the results across these images matched closely with the overall results of each method, so as to be best indicative of the performance differences between models.

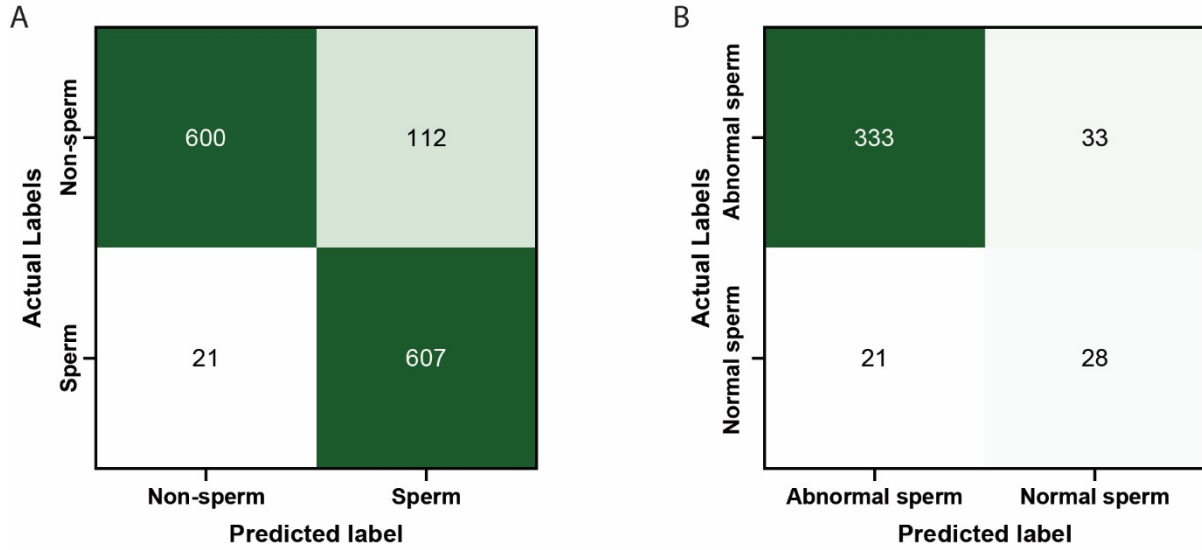


Supplementary Figure 8 | Sampled images from the embryo dataset (ED1) as evaluated by different domain adaption approaches. The networks were trained to classify between the blastocyst and non-blastocyst embryo images using labelled ED4 and unlabelled ED1 training data

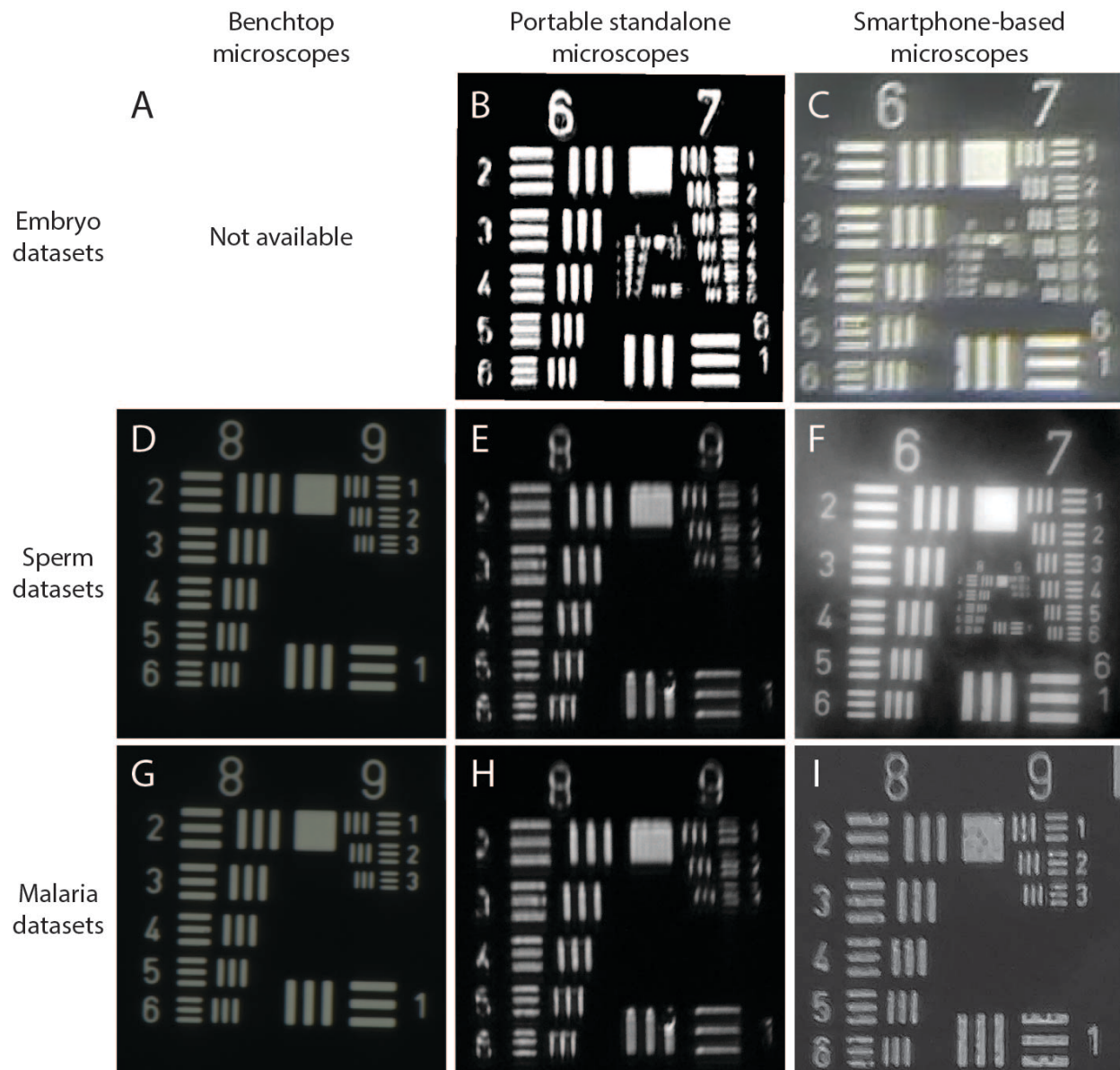
and the best performing models were used in evaluating the sampled images. The images were sampled from ED1 test dataset such that the results across these images matched closely with the overall results of each method, so as to be best indicative of the performance differences between models.



Supplementary Figure 9 | Data structure of sperm images utilised in the development and evaluation of the neural networks. Source data used for training and testing was annotated by expert clinical staff. Patient test (SD4) and all other datasets (SD3, SD2, and SD1) were not annotated.



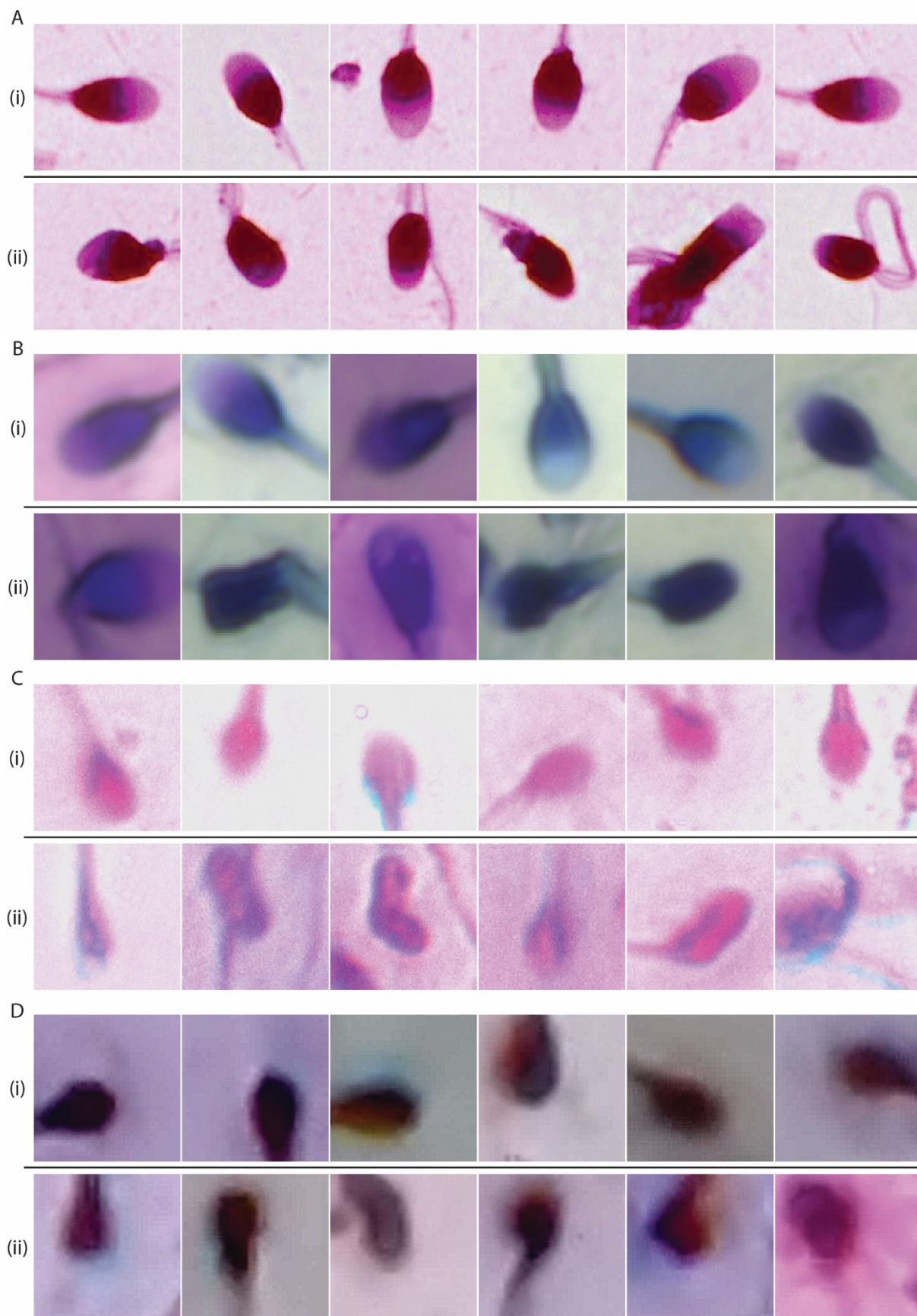
Supplementary Figure 10 | Confusion matrices of MD-nets in the evaluation of sperm images collected using high-resolution microscopes (SD4). (A) The matrix represents the confusion of a trained neural network used in classifying images between sperm and non-sperm cells during initial filtering (n=1340). (B) The confusion of the base MD-net algorithm in differentiating between sperm of normal and abnormal morphological quality (n=415).



Supplementary Figure 11 | Resolving power tests using the USAF 1951 resolution target. (A)

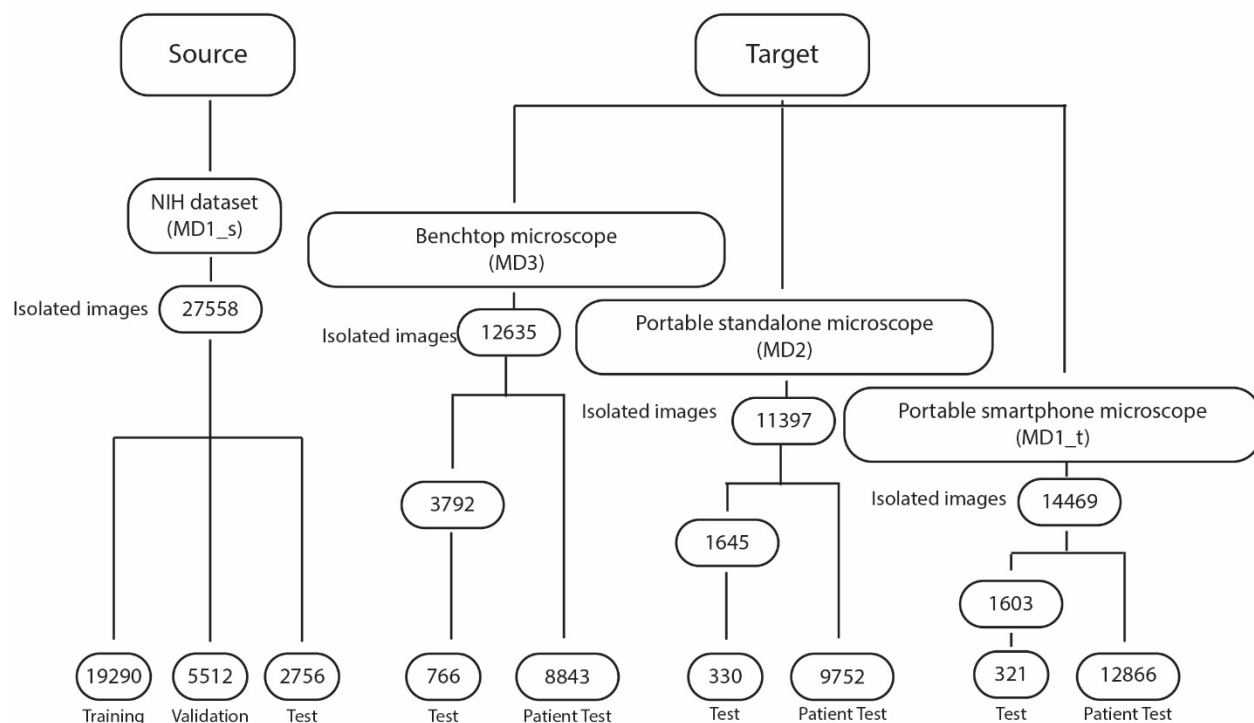
Since the embryo data was collected using multiple imaging systems at different fertility centers, the resolving power of those microscopes was not known to us. (B) The resolving power of the 3D-printed portable optical system used for imaging embryos was $4.38 \mu\text{m}$ ($\sim 114 \text{ lp/mm}$). (C) The resolving power of the smartphone-based optical system used for imaging embryos was $3.1 \mu\text{m}$ ($\sim 161 \text{ lp/mm}$). (D) The resolving power of the benchtop microscope used for imaging sperm was $<0.78 \mu\text{m}$ ($>912 \text{ lp/mm}$). (E) The resolving power of the 3D-printed portable optical system used

for imaging sperm was $0.98 \mu\text{m}$ ($\sim 512 \text{ lp/mm}$). (F) The resolving power of the smartphone-based optical system used for imaging sperm was $1.74 \mu\text{m}$ ($\sim 287 \text{ lp/mm}$). (G) The resolving power of the benchtop microscope used for imaging red blood cells (RBCs) for malaria was $<0.78 \mu\text{m}$ ($>912 \text{ lp/mm}$). (H) The resolving power of the 3D-printed portable optical system used for imaging RBCs for malaria was $0.98 \mu\text{m}$ ($\sim 512 \text{ lp/mm}$). (I) The resolving power of the smartphone-based microscope used for imaging RBCs for malaria detection was $<0.78 \mu\text{m}$ ($>912 \text{ lp/mm}$).



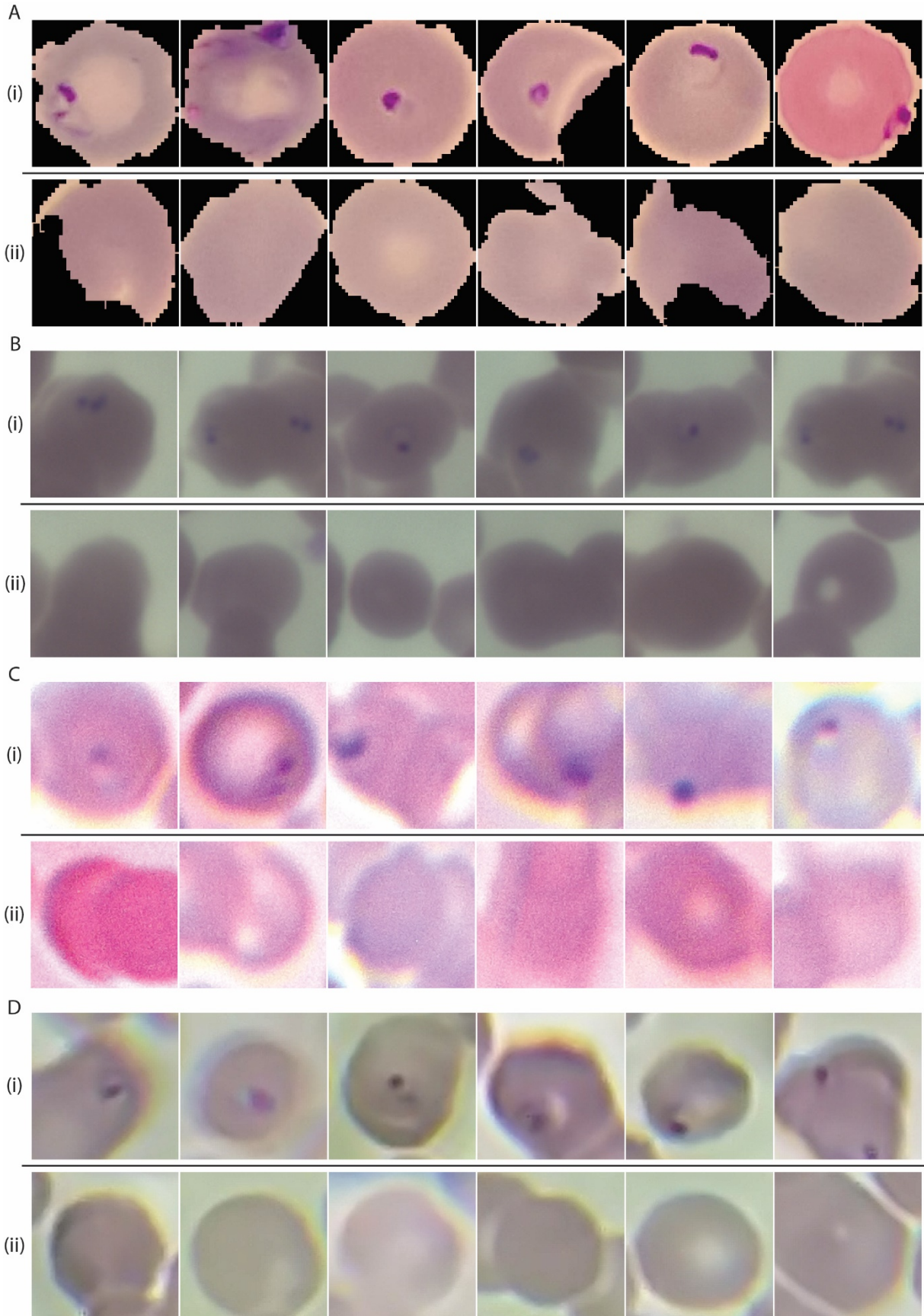
Supplementary Figure 12 | Sampled images from the sperm datasets. MD-nets were trained to differentiate between sperm of normal and abnormal morphological qualities. (A) SD4 images collected using high-resolution microscopy by the American Association of Bioanalysts. MD-net was trained using labelled and unlabelled SD4 data. Example SD4 sperm images, which were reported by the expert annotators and MD-nets as sperm of (i) normal and (ii) abnormal morphologies. (B) SD3 images were collected using a benchtop microscope. MD-net was trained using labelled SD4 and unlabelled SD3 data. Example SD3 images of sperm which were considered by MD-nets as sperm of (i) normal and (ii) abnormal morphologies. (C) SD2 images collected using a 3D-printed portable microscope. MD-net was trained using labelled SD4 and unlabelled SD2 data. Example SD2 images of sperm which were considered by MD-nets as sperm of (i) normal and (ii) abnormal morphologies. (D) SD1 images were collected using an inexpensive smartphone-based microscope. MD-net was trained using labelled SD4 and unlabelled SD1 training data. Example SD1 images of sperm which were considered by MD-nets as sperm of (i) normal and (ii) abnormal morphologies.

Malaria Data Structure

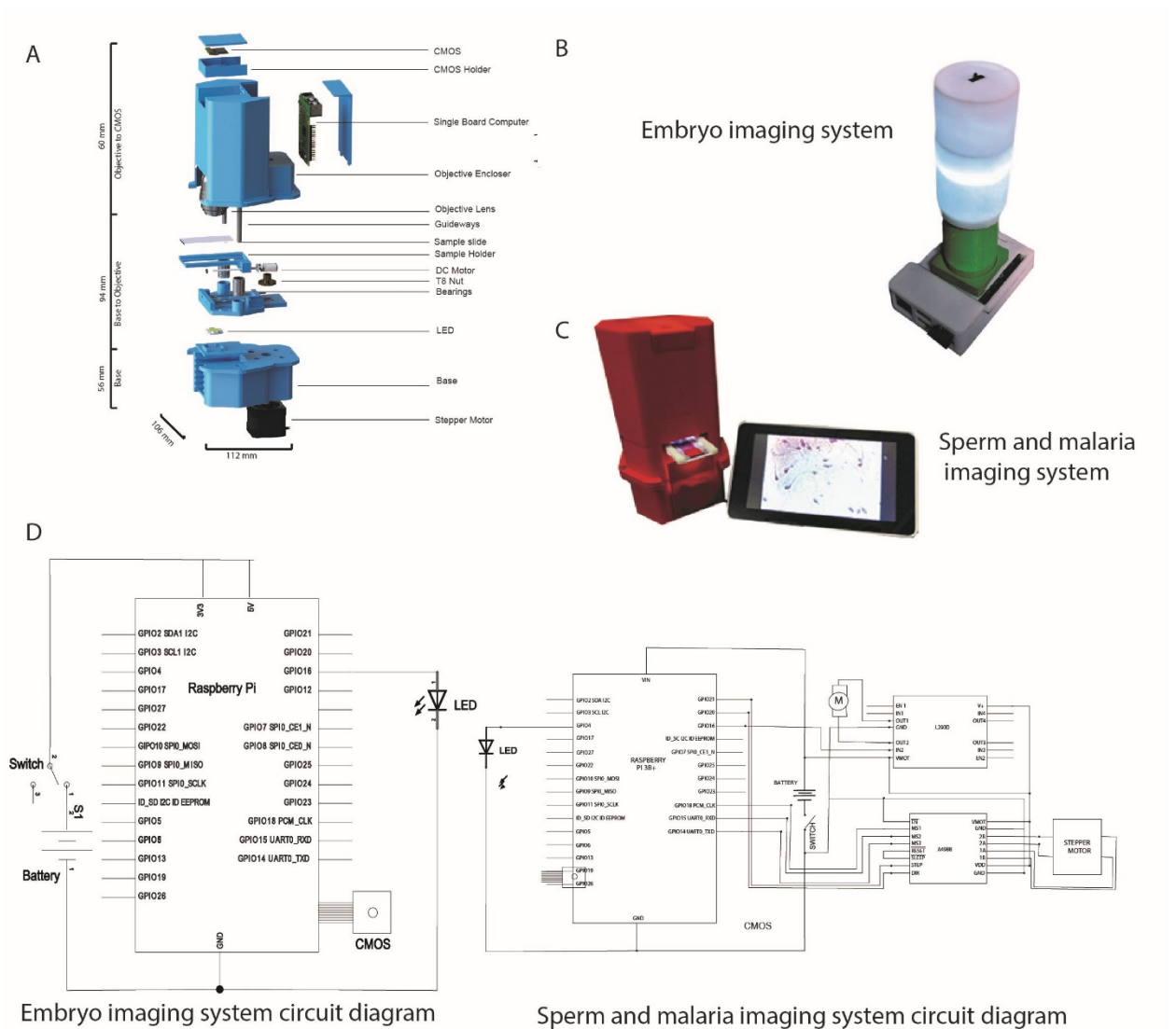


Supplementary Figure 13 | Data structure of malaria-infected and non-infected blood cell images utilised in the development and evaluation of the neural networks. Source data made use of annotations that were available with a public dataset. All other image data was annotated by lab staff.

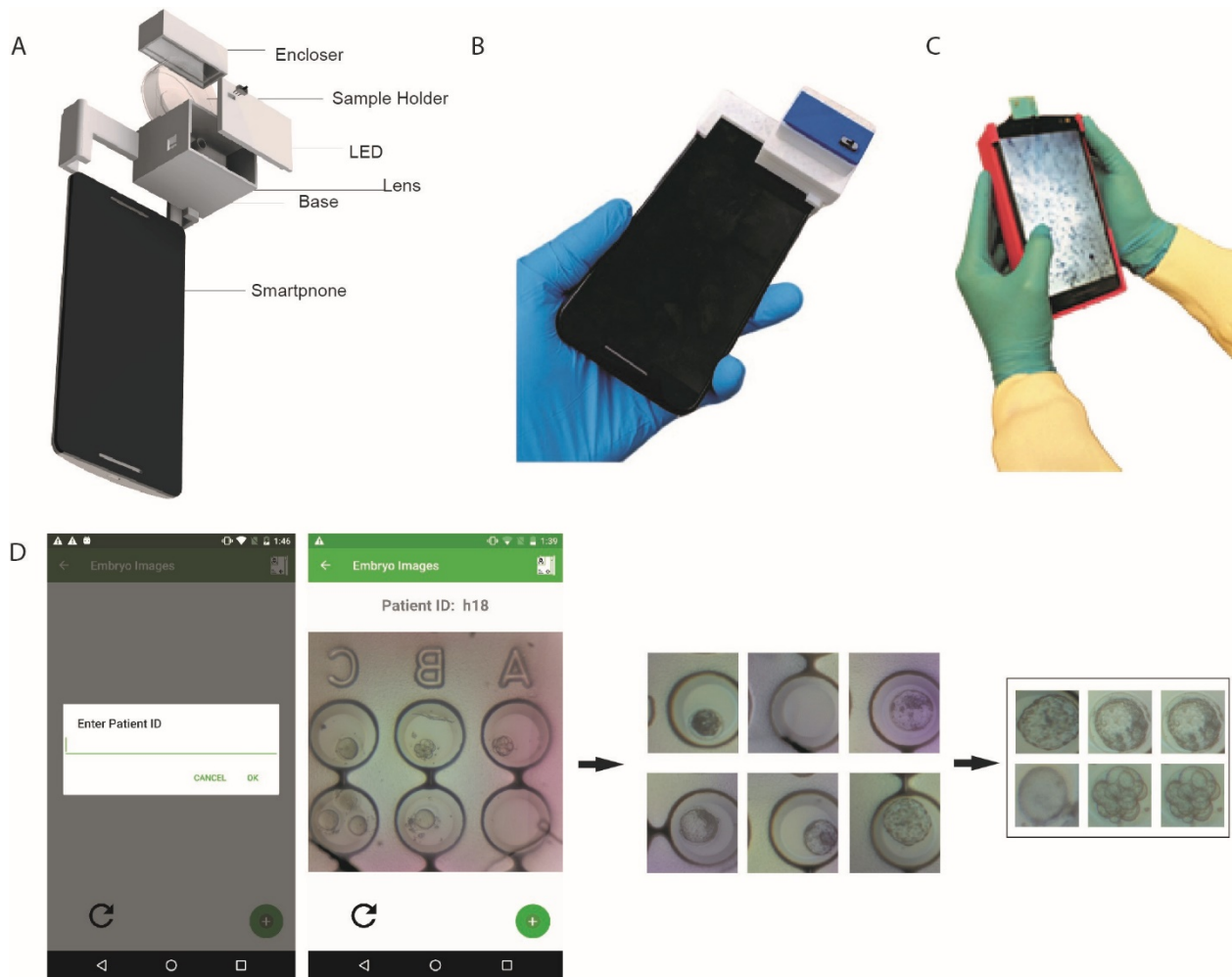
illustrating source and target clustering achieved by MD-net SW when trained with limited source data for different blood cell datasets.



Supplementary Figure 15 | Sampled images from the malaria datasets. MD-nets were trained to differentiate between parasitised and non-parasitised RBCs. (A) MD1_s images collected using a smartphone camera attached to a benchtop brightfield microscope for the NIH Malaria Screener research study. A ResNet-50 classifier was developed through supervised learning using MD1_s data. Example MD1_s RBC images which were reported by the expert annotators and the ResNet-50 classifier as (i) parasitised and (ii) non-parasitised RBCs. (B) MD3 images collected using a benchtop microscope. MD-net (NoS) was trained using unlabelled MD3 data, with the pretrained network weights from the ResNet-50 model trained using MD1_s data. Example MD3 images of RBCs which were considered by MD-net (NoS) and the expert annotators as (i) parasitised and (ii) non-parasitised RBCs. (C) MD2 images collected using a 3D-printed portable microscope. MD-net (NoS) was trained using unlabelled MD2 data, with the pretrained network weights from the ResNet-50 model trained using MD1_s data. Example MD2 images of RBCs which were considered by MD-net (NoS) and the expert annotators as (i) parasitised and (ii) non-parasitised RBCs. (D) MD1_t images collected using a smartphone attached to a benchtop microscope. MD-net (NoS) was trained using unlabelled MD1_t data, with the pretrained network weights from the ResNet-50 model trained using MD1_s data. Example MD1_t images of RBCs which were considered by MD-net (NoS) and the expert annotators as (i) parasitised and (ii) non-parasitised RBCs.

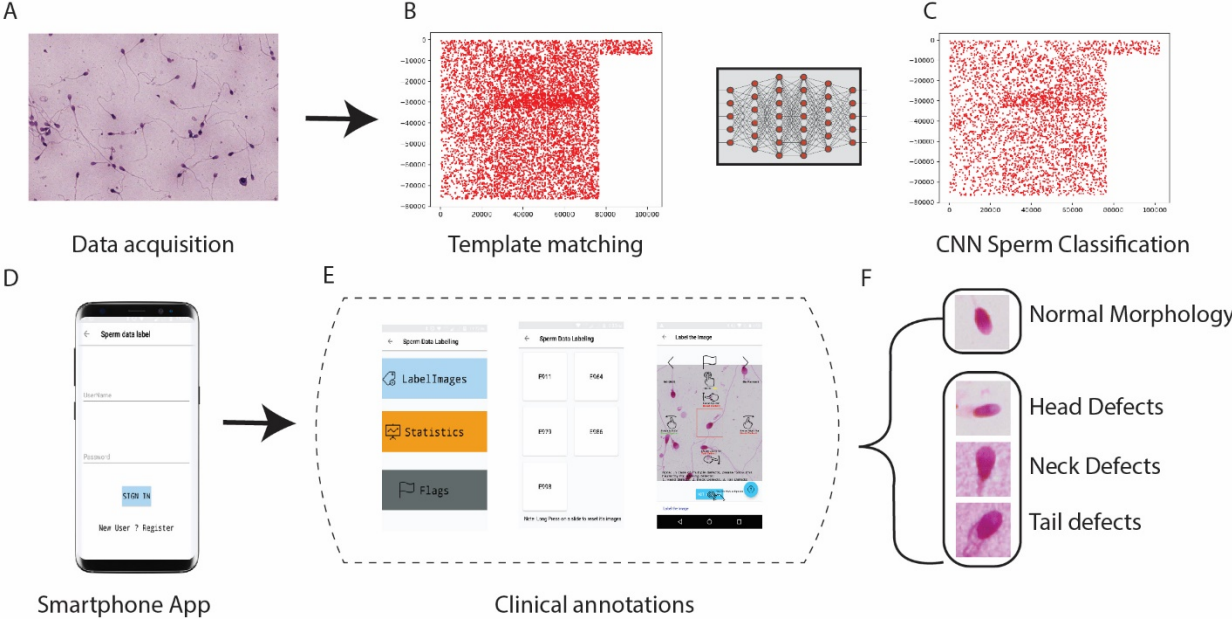


Supplementary Figure 16 | Portable standalone 3D-printed imaging systems. (A) The exploded image shows various components of the automated portable standalone imaging system used for sperm and malaria dataset collection (SD2 and MD2). The embryo imaging system did not possess any mechanical automation. (B) An image of the 3D-printed optical system used for the collection of embryo image dataset (ED2) (C) An image of the 3D-printed optical system used for the collection of sperm and malaria image datasets (SD2 and MD2) (D) The circuit diagram showing various electrical components of the two imaging systems.

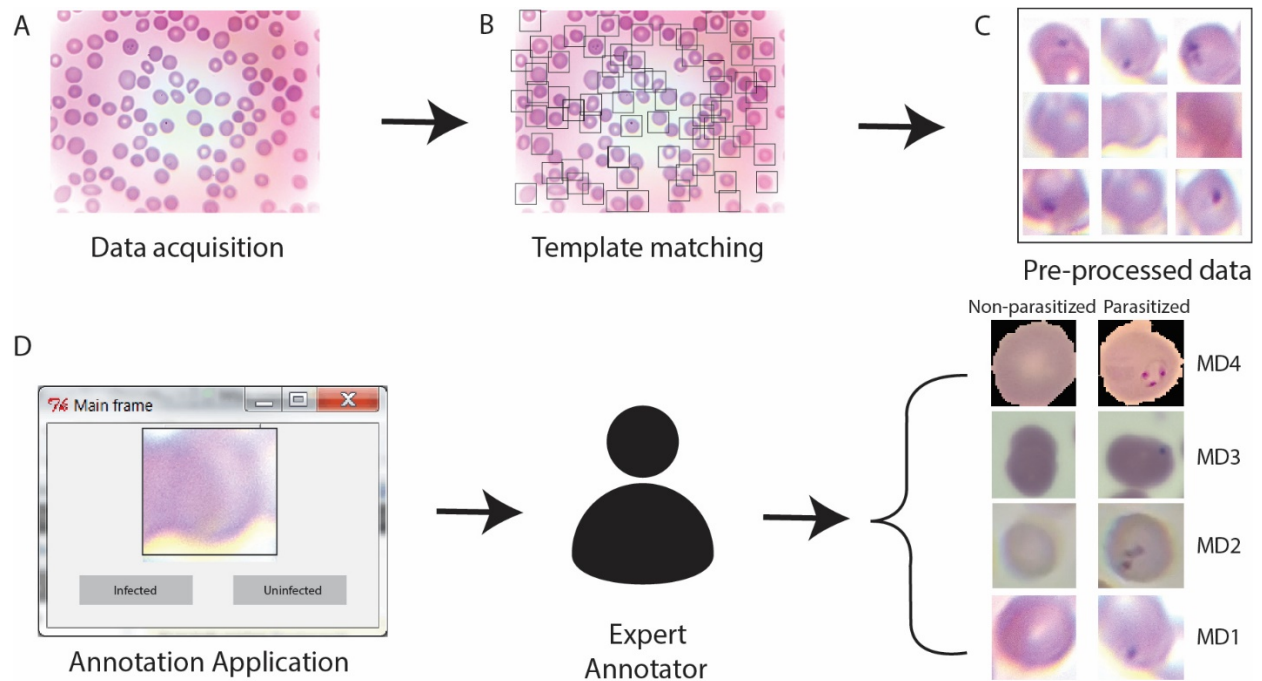


Supplementary Figure 17 | 3D-printed smartphone-based imaging systems. (A) The exploded image shows various components of the smartphone-based imaging system. The embryo imaging system used the front camera of a smartphone while the sperm imaging system used the rear camera. (B) An image of the 3D-printed smartphone-based imaging system used for the collection of embryo image dataset (ED1). (C) An image of the 3D-printed smartphone-based imaging system used for the collection of sperm image dataset (SD1). (D) The smartphone application interface developed for imaging embryos and process flow of image collection. The smartphone

application uses a simple camera interface for capturing images of multi-welled embryo dishes. A template matching algorithm was used to isolate individual wells and identifiers. These images were then cropped/resized prior to their use in training/testing the neural networks.



Supplementary Figure 18 | Sperm data collection and annotation process flow. (A) Sperm samples were stained and imaged using the optical systems used in this study. (B) The images containing multiple sperm cells were initially processed using a template matching algorithm to identify sperm-like objects for classification. (C) The objects were then filtered using a neural network classifier that was trained to differentiate between sperm and non-sperm images. (D) and (E) A smartphone application was developed to help expert labeling. (F) The filtered sperm images were annotated as normal and abnormal sperm morphology (head, neck, and tail defects).



Supplementary Figure 19 | Malaria data collection and annotation process flow. (A) Thin-blood smears were stained and imaged using the optical systems used in this study. (B) and (C) The images were processed using a template matching algorithm to identify red blood cells for classification. (D) The isolated images were annotated using a simple annotation tool, built in-house on Python, to identify infected and non-infected RBCs. The annotated images were used in training and testing the developed networks.

Supplementary Table 1 | Performance of the best tuned MD-net models on embryo datasets.

The best performing MD-net models used the Xception architecture.

Adversarial network performance	ED4 (n=742)	ED3 (n=258)	ED2 (n=69)	ED1 (n=296)
Accuracy	92.32%	98.84%	95.65%	97.64%
Sensitivity	92.67%	100.00%	94.64%	98.48%
Specificity	91.63%	97.87%	100.00%	95.96%
Positive predictive value	86.47%	97.50%	100.00%	97.98%
Negative predictive value	92.67%	100%	81.25%	96.94%

Supplementary Table 2 | Performance of different MD-net and supervised learning models

on embryo datasets. Each architecture was first fine-tuned, and the hyperparameters of the best performing model were used for this section of the study. Different seeds were used to initialise the best performing models.

<i>ED4</i>						
<i>Multilayer-CNN</i>	Seed	Accuracy	TPR	TNR	PPV	NPV
	884	84.64	87.58	78.88	89.03	76.45
	2004	84.5	84.32	84.86	91.59	73.45
	3118	82.48	83.3	80.88	89.5	71.23
	5918	82.08	83.3	79.68	88.91	70.92
	8468	84.91	86.15	82.47	90.58	75.27
	Average	83.72	84.93	81.35	89.92	73.46
<i>Inception</i>	Seed	Accuracy	TPR	TNR	PPV	NPV
	884	83.15	76.37	96.41	97.66	67.6
	2004	83.42	77.19	95.62	97.18	68.18
	3118	83.69	76.99	96.81	97.93	68.26
	5918	82.08	74.13	97.61	98.38	65.86
	8468	82.61	79.43	88.84	93.3	68.83
	Average	82.99	76.82	95.06	96.89	67.75
<i>ResNet-50</i>	Seed	Accuracy	TPR	TNR	PPV	NPV
	884	88.54	86.15	93.23	96.14	77.48
	2004	89.62	87.78	93.23	96.21	79.59
	3118	88.81	90.22	86.06	92.68	81.82
	5918	90.43	90.02	91.24	95.26	82.37
	8468	88.95	88.39	90.04	94.55	79.86

	Average	89.27	88.51	90.76	94.97	80.22	
<i>Xception</i>	Seed	Accuracy	TPR	TNR	PPV	NPV	
	884	90.7	92.26	87.65	93.6	85.27	
	2004	89.76	90.43	88.45	93.87	82.53	
	8468	89.76	89.82	89.64	94.43	81.82	
	3118	89.08	88.8	89.64	94.37	80.36	
	5918	89.62	89.61	89.64	94.42	81.52	
<i>Inception ResNet V2</i>	Average	89.78	90.18	89	94.14	82.3	
	Seed	Accuracy	TPR	TNR	PPV	NPV	
	884	83.96	78	95.62	97.21	68.97	
	2004	82.48	75.15	96.81	97.88	66.58	
	3118	83.29	76.17	97.21	98.16	67.59	
	5918	87.47	84.52	93.23	96.06	75.48	
<i>MD-nets</i>	8468	86.79	84.73	90.84	94.76	75.25	
	Average	84.8	79.71	94.74	96.81	70.77	
	Seed	Accuracy	TPR	TNR	PPV	NPV	
	1	91.11	91.85	89.64	94.55	84.91	
	1000	90.7	91.45	89.24	94.33	84.21	
	10000	91.24	91.85	90.04	94.75	84.96	
<i>ED3</i>	10	92.18	92.87	90.84	95.2	86.69	
	0	92.32	92.67	91.63	95.59	86.47	
	Average	91.51	92.14	90.28	94.88	85.45	
	<i>Multilayer-CNN</i>	Seed	Accuracy	TPR	TNR	PPV	NPV
		884	52.33	80.34	29.08	48.45	64.06
		2004	45.74	85.47	12.77	44.84	51.43
3118		57.75	76.92	41.84	52.33	68.6	
5918		60.85	64.96	57.45	55.88	66.39	
8468		63.57	39.32	83.69	66.67	62.43	
<i>Inception</i>	Average	56.05	69.4	44.97	53.63	62.58	
	Seed	Accuracy	TPR	TNR	PPV	NPV	
	884	94.19	88.03	99.29	99.04	90.91	
	2004	76.74	48.72	100	100	70.15	
	3118	90.7	80.34	99.29	98.95	85.89	
	5918	88.76	76.07	99.29	98.89	83.33	
<i>ResNet-50</i>	8468	91.09	80.34	100	100	85.98	
	Average	88.3	74.7	99.57	99.38	83.25	
	Seed	Accuracy	TPR	TNR	PPV	NPV	
	884	87.6	78.63	95.04	92.93	84.28	
	2004	88.76	92.31	85.82	84.38	93.08	
	3118	93.02	90.6	95.04	93.81	92.41	
	5918	80.62	81.2	80.14	77.24	83.7	

	8468	82.56	87.18	78.72	77.27	88.1
	Average	86.51	85.98	86.95	85.13	88.31
<i>Xception</i>	Seed	Accuracy	TPR	TNR	PPV	NPV
	884	92.64	94.87	90.78	89.52	95.52
	2004	68.99	98.29	44.68	59.59	96.92
	8468	91.09	96.58	86.52	85.61	96.83
	3118	77.13	98.29	59.57	66.86	97.67
	5918	74.03	98.29	53.9	63.89	97.44
	Average	80.78	97.26	67.09	73.09	96.88
<i>Inception ResNet V2</i>	Seed	Accuracy	TPR	TNR	PPV	NPV
	884	87.6	72.65	100	100	81.5
	2004	84.88	70.09	97.16	95.35	79.65
	3118	91.09	88.89	92.91	91.23	90.97
	5918	89.15	78.63	97.87	96.84	84.66
	8468	86.05	69.23	100	100	79.66
	Average	87.75	75.9	97.59	96.68	83.29
<i>MD-nets</i>	Seed	Accuracy	TPR	TNR	PPV	NPV
	1	98.84	100	97.87	97.5	100
	1000	98.84	100	97.87	97.5	100
	10000	98.84	100	97.87	97.5	100
	10	98.06	99.15	97.16	96.67	99.28
	0	98.84	100	97.87	97.5	100
	Average	98.68	99.83	97.73	97.33	99.86
ED2						
<i>Multilayer-CNN</i>	Seed	Accuracy	TPR	TNR	PPV	NPV
	884	57.97	53.57	76.92	90.91	27.78
	2004	69.57	73.21	53.85	87.23	31.82
	3118	49.28	42.86	76.92	88.89	23.81
	5918	39.13	25	100	100	23.64
	8468	24.64	7.14	100	100	20
	Average	48.12	40.36	81.54	93.41	25.41
<i>Inception</i>	Seed	Accuracy	TPR	TNR	PPV	NPV
	884	81.16	96.43	15.38	83.08	50
	2004	76.81	80.36	61.54	90	42.11
	3118	84.06	96.43	30.77	85.71	66.67
	5918	75.36	83.93	38.46	85.45	35.71
	8468	85.51	91.07	61.54	91.07	61.54
	Average	80.58	89.64	41.54	87.06	51.21
<i>ResNet-50</i>	Seed	Accuracy	TPR	TNR	PPV	NPV
	884	79.71	94.64	15.38	82.81	40
	2004	75.36	78.57	61.54	89.8	40
	3118	82.61	100	7.69	82.35	100

	5918	81.16	98.21	7.69	82.09	50
	8468	82.61	100	7.69	82.35	100
	Average	80.29	94.28	20	83.88	66
<i>Xception</i>	Seed	Accuracy	TPR	TNR	PPV	NPV
	884	89.86	100	46.15	88.89	100
	2004	81.16	100	0	81.16	-
	8468	84.06	100	15.38	83.58	100
	3118	79.71	98.21	0	80.88	0
	5918	81.16	100	0	81.16	-
	Average	83.19	99.64	12.31	83.13	66.67
<i>Inception ResNet V2</i>	Seed	Accuracy	TPR	TNR	PPV	NPV
	884	86.96	91.07	69.23	92.73	64.29
	2004	86.96	96.43	46.15	88.52	75
	3118	84.06	98.21	23.08	84.62	75
	5918	86.96	94.64	53.85	89.83	70
	8468	60.87	57.14	76.92	91.43	29.41
	Average	81.16	87.5	53.85	89.43	62.74
<i>MD-nets</i>	Seed	Accuracy	TPR	TNR	PPV	NPV
	1	94.2	94.64	92.31	98.15	80
	1000	91.3	96.43	69.23	93.1	81.82
	10000	94.2	96.43	84.62	96.43	84.62
	10	94.2	94.64	92.31	98.15	80
	0	95.65	94.64	100	100	81.25
	Average	93.91	95.36	87.69	97.17	81.54
EDI						
<i>Multilayer-CNN</i>	Seed	Accuracy	TPR	TNR	PPV	NPV
	884	43.24	14.72	100	100	37.08
	2004	53.38	34.01	91.92	89.33	41.18
	3118	45.27	17.77	100	100	37.93
	5918	36.82	5.08	100	100	34.62
	8468	35.81	3.55	100	100	34.26
	Average	42.9	15.03	98.38	97.87	37.01
<i>Inception</i>	Seed	Accuracy	TPR	TNR	PPV	NPV
	884	80.07	80.2	79.8	88.76	66.95
	2004	56.76	46.19	77.78	80.53	42.08
	3118	77.03	94.42	42.42	76.54	79.25
	5918	80.74	82.23	77.78	88.04	68.75
	8468	63.18	50.76	87.88	89.29	47.28
	Average	71.56	70.76	73.13	84.63	60.86
<i>ResNet-50</i>	Seed	Accuracy	TPR	TNR	PPV	NPV
	884	65.88	98.48	1.01	66.44	25
	2004	33.45	30.96	38.38	50	21.84

	3118	61.49	91.88	1.01	64.87	5.88
	5918	49.32	51.78	44.44	64.97	31.65
	8468	61.15	91.88	0	64.64	0
	Average	54.26	73	16.97	62.18	16.87
<i>Xception</i>	Seed	Accuracy	TPR	TNR	PPV	NPV
	884	82.43	88.32	70.71	85.71	75.27
	2004	67.23	100	2.02	67.01	100
	8468	67.91	100	4.04	67.47	100
	3118	66.55	100	0	66.55	-
	5918	67.23	100	2.02	67.01	100
	Average	70.27	97.66	15.76	70.75	93.82
<i>Inception ResNet V2</i>	Seed	Accuracy	TPR	TNR	PPV	NPV
	884	78.04	73.1	87.88	92.31	62.14
	2004	72.3	65.48	85.86	90.21	55.56
	3118	76.69	88.32	53.54	79.09	69.74
	5918	73.31	70.05	79.8	87.34	57.25
	8468	69.93	64.47	80.81	86.99	53.33
	Average	74.05	72.28	77.58	87.19	59.6
<i>MD-nets</i>	Seed	Accuracy	TPR	TNR	PPV	NPV
	1	97.3	100	91.92	96.1	100
	1000	96.28	97.46	93.94	96.97	94.9
	10000	94.26	93.91	94.95	97.37	88.68
	10	95.95	100	87.88	94.26	100
	0	97.64	98.48	95.96	97.98	96.94
	Average	96.28	97.97	92.93	96.54	96.1

Supplementary Table 3 | Performance of different domain adaption approaches on Office-

31. All values are reported as the average of 5 randomly seeded 3-cross validation tests.

Approaches marked by an asterisk were implemented in this study. The values of all other approaches were reported previously by others. Error bars represent the standard error of the mean.

OFFICE 31 dataset	A → W	D → W	W → D	A → D	D → A	W → A	Average
Source only (ResNet50) *	76.4 ± 1.2	96.1 ± 0.3	99.1 ± 0.2	79.9 ± 1.0	62.1 ± 0.3	65.3 ± 1.2	79.8
ADDA	86.2 ± 0.5	96.2 ± 0.3	98.4 ± 0.3	77.8 ± 0.3	69.5 ± 0.4	68.9 ± 0.5	82.9
DANN	82.0 ± 0.4	96.9 ± 0.2	99.1 ± 0.1	79.7 ± 0.4	68.2 ± 0.4	67.4 ± 0.5	82.2
DAN	80.5 ± 0.4	97.1 ± 0.2	99.6 ± 0.1	78.6 ± 0.2	63.6 ± 0.3	62.8 ± 0.2	80.4
PixelDA *	5.6 ± 1.2	17.1 ± 13.1	19.5 ± 10.7	10.8 ± 1.1	5.5 ± 2.1	5.6 ± 2.2	10.6
CAN	94.5 ± 0.3	99.1 ± 0.2	99.8 ± 0.2	95.0 ± 0.3	78.0 ± 0.3	77.0 ± 0.3	90.6
CDAN	94.1 ± 0.1	98.6 ± 0.1	100 ± 0	92.9 ± 0.2	71.0 ± 0.3	69.3 ± 0.3	87.7
GAGL *	73.8 ± 1.5	97.8 ± 0.4	98.5 ± 0.2	76.2 ± 2.9	59.4 ± 1.2	60.2 ± 2.0	77.7
MD-nets *	95.2 ± 0.5	99.2 ± 0.04	100 ± 0	94.2 ± 0.3	77.2 ± 0.3	78.2 ± 0.2	90.7
MD-net NoS *	92.9 ± 0.2	98.5 ± 0.04	99.6 ± 0.2	91.8 ± 0.1	72.6 ± 0.4	74.8 ± 0.2	88.4

Supplementary Table 4 | 2-class performance of different domain adaption approaches on

the Embryo dataset. Hyperparameter optimisations were performed and the best model results were reported. Error bars represent the standard error of the mean (n = 5 seeds).

Embryo dataset	2-class Accuracy				Average
	ED4 → ED4	ED4 → ED3	ED4 → ED2	ED4 → ED1	
Source only (ResNet50)	89.3 ± 0.8	86.5 ± 2.2	80.3 ± 1.3	54.3 ± 5.9	77.6
DANN	90.6 ± 0.2	97.2 ± 0.4	46.1 ± 8.3	79.9 ± 1.7	78.4
PIXELDA	65.3 ± 0.9	72.9 ± 6.7	61.2 ± 11.6	57.9 ± 6.9	64.3
CAN	84.6 ± 3.1	99.5 ± 0.1	62.6 ± 11	89.3 ± 5.1	84.0
ADDA	90.7 ± 0	94 ± 0.8	57.1 ± 7.2	86.6 ± 0.9	82.1
GAGL	89.1 ± 0.5	81.1 ± 3	91.6 ± 1.6	78.7 ± 2.3	85.1
MD-nets (ResNet50)	91.1 ± 0.5	99.1 ± 0.2	87.4 ± 2.7	91.1 ± 1.2	92.2
Source only (Xception)	89.8 ± 0.6	80.8 ± 4.7	83.2 ± 1.8	70.3 ± 3	81.0
MD-nets (Xception)	91.5 ± 0.3	98.7 ± 0.2	93.9 ± 0.7	96.3 ± 0.6	95.1

Supplementary Table 5 | Model-specific dataset splits used in the development and evaluation of different domain adaption methods reported in this study. The source validation datasets were split from the training data and the target validation datasets were sampled from the target data.

Method	Base network	Model ID	Source - Training	Source(S)/Target(T) Validation	Target Test	Secondary Test
GAGL	ResNet-50	A -> D	2524	66 (T)	498	N/A
MD-nets	ResNet-50	A -> D	2524	293 (S)	498	N/A
MD-nets (NoS)	ResNet-50	A -> D	N/A	66 (T)	498	N/A
PIXELDA	ResNet-50	A -> D	2524	66 (T)	498	N/A
GAGL	ResNet-50	A -> W	2524	91 (T)	795	N/A
MD-nets	ResNet-50	A -> W	2524	293 (S)	795	N/A
MD-nets (NoS)	ResNet-50	A -> W	N/A	91 (T)	795	N/A
PIXELDA	ResNet-50	A -> W	2524	91 (T)	795	N/A
GAGL	ResNet-50	D -> A	432	293 (T)	2817	N/A
MD-nets	ResNet-50	D -> A	432	66 (S)	2817	N/A
MD-nets (NoS)	ResNet-50	D -> A	N/A	293 (T)	2817	N/A
PIXELDA	ResNet-50	D -> A	432	293 (T)	2817	N/A
GAGL	ResNet-50	D -> W	432	91 (T)	795	N/A
MD-nets	ResNet-50	D -> W	432	66 (S)	795	N/A
MD-nets (NoS)	ResNet-50	D -> W	N/A	91 (T)	795	N/A
PIXELDA	ResNet-50	D -> W	432	91 (T)	795	N/A
GAGL	ResNet-50	W -> A	704	293 (T)	2817	N/A
MD-nets	ResNet-50	W -> A	704	91 (S)	2817	N/A
MD-nets (NoS)	ResNet-50	W -> A	N/A	293 (T)	2817	N/A
PIXELDA	ResNet-50	W -> A	704	293 (T)	2817	N/A
GAGL	ResNet-50	W -> D	704	66 (T)	498	N/A
MD-nets	ResNet-50	W -> D	704	91 (S)	498	N/A
MD-nets (NoS)	ResNet-50	W -> D	N/A	66 (T)	498	N/A
PIXELDA	ResNet-50	W -> D	704	66 (T)	498	N/A
ADDA	ResNet-50	EM4	1188	74 (T)	742	N/A
CAN	ResNet-50	EM4	1188	N/A	742	N/A
DANN	ResNet-50	EM4	1188	510 (S)	742	N/A
GAGL	ResNet-50	EM4	1188	74 (T)	742	N/A
MD-nets	Xception	EM4	1188	510 (S)	742	N/A
MD-nets	ResNet-50	EM4	1188	510 (S)	742	N/A
PIXELDA	ResNet-50	EM4	1188	74 (T)	742	N/A
ADDA	ResNet-50	EM41	1930	29 (T)	296	N/A
CAN	ResNet-50	EM41	1930	N/A	296	N/A

DANN	ResNet-50	EM41	1930	510 (S)	296	N/A
GAGL	ResNet-50	EM41	1930	29 (T)	296	N/A
MD-nets	Xception	EM41	1930	510 (S)	296	N/A
MD-nets	ResNet-50	EM41	1930	510 (S)	296	N/A
PIXELDA	ResNet-50	EM41	1930	29 (T)	296	N/A
ADDA	ResNet-50	EM42	1930	6 (T)	69	N/A
CAN	ResNet-50	EM42	1930	N/A	69	N/A
DANN	ResNet-50	EM42	1930	510 (S)	69	N/A
GAGL	ResNet-50	EM42	1930	6 (T)	69	N/A
MD-nets	Xception	EM42	1930	510 (S)	69	N/A
MD-nets	ResNet-50	EM42	1930	510 (S)	69	N/A
PIXELDA	ResNet-50	EM42	1930	6 (T)	69	N/A
ADDA	ResNet-50	EM43	1930	25 (T)	258	N/A
CAN	ResNet-50	EM43	1930	N/A	258	N/A
DANN	ResNet-50	EM43	1930	510 (S)	258	N/A
GAGL	ResNet-50	EM43	1930	25 (T)	258	N/A
MD-nets	Xception	EM43	1930	510 (S)	258	N/A
MD-nets	ResNet-50	EM43	1930	510 (S)	258	N/A
PIXELDA	ResNet-50	EM43	1930	25 (T)	258	N/A
MD-nets (NoS)	ResNet-50	MM(nos)1_t	N/A	129 (T)	1282	321
MD-nets (NoS)	ResNet-50	MM(nos)2	N/A	131 (T)	1315	330
MD-nets (NoS)	ResNet-50	MM(nos)3	N/A	302 (T)	3026	766
MD-nets	ResNet-50	MM1_s1_t	19290	5512 (S)	1282	321
MD-nets	ResNet-50	MM1_s2	19290	5512 (S)	1315	330
MD-nets	ResNet-50	MM1_s3	19290	5512 (S)	3026	766
MD-nets (SW)	ResNet-50	MM1_s1_t	5512	2756 (S)	1282	321
MD-nets (SW)	ResNet-50	MM1_s2	5512	2756 (S)	1315	330
MD-nets (SW)	ResNet-50	MM1_s3	5512	2756 (S)	3026	766
MD-nets	Xception	SM4	2899	828 (S)	415	193141
MD-nets	Xception	SM41	3312	830 (S)	20554	N/A
MD-nets	Xception	SM42	3312	830 (S)	19668	N/A
MD-nets	Xception	SM43	3312	830 (S)	100892	N/A

Supplementary Table 6 | Hyperparameters of the best performing domain adaption models.

All models used a Nesterov momentum of 0.9, an inverse time decay learning rate scheduler, and SGD optimiser. ADAM optimisers were also evaluated. MM(nos)2 utilised a step decay scheduler. Lowest target validation loss (TVL) and source validation loss (SVL) were used in stopping and selecting the best models. Loss values were monitored for every iteration (itr). The batch sizes listed in bold are the batch sizes used for the best performing models.

Model	Base Network	Model ID/Task	Learning rate range	Best Learning Rate	Weight Decay	Batch sizes	Input size (pixels)	Stoppage criteria	Patience (itr)
GAGL	ResNet-50	A -> D	(0.001-0.0001)	0.0005	0.0005	32,64	224X224	min(TVL)	5000
MD-nets	ResNet-50	A -> D	(0.001-0.0001)	0.0003	0.0005	32,64	224X224	min(SVL)	5000
MD-nets (NoS)	ResNet-50	A -> D	(0.001-0.0001)	0.0001	0.001	32,64	224X224	min(TVL)	5000
PIXELDA	ResNet-50	A -> D	(0.001-0.0001)	0.0001	N/A	32,64	224X224	min(TVL)	N/A
GAGL	ResNet-50	A -> W	(0.001-0.0001)	0.001	0.0005	32,64	224X224	min(TVL)	5000
MD-nets	ResNet-50	A -> W	(0.001-0.0001)	0.001	0.0005	32,64	224X224	min(SVL)	5000
MD-nets (NoS)	ResNet-50	A -> W	(0.001-0.0001)	0.001	0.001	32,64	224X224	min(TVL)	5000
PIXELDA	ResNet-50	A -> W	(0.001-0.0001)	0.0005	N/A	32,64	224X224	min(TVL)	N/A
GAGL	ResNet-50	D -> A	(0.001-0.0001)	0.001	0.0005	32,64	224X224	min(TVL)	5000
MD-nets	ResNet-50	D -> A	(0.001-0.0001)	0.001	0.0005	32,64	224X224	min(SVL)	5000
MD-nets (NoS)	ResNet-50	D -> A	(0.001-0.0001)	0.0001	0.001	32,64	224X224	min(TVL)	5000
PIXELDA	ResNet-50	D -> A	(0.001-0.0001)	0.0005	N/A	32,64	224X224	min(TVL)	N/A
GAGL	ResNet-50	D -> W	(0.001-0.0001)	0.0005	0.0005	32,64	224X224	min(TVL)	5000
MD-nets	ResNet-50	D -> W	(0.001-0.0001)	0.0003	0.0005	32,64	224X224	min(SVL)	5000
MD-nets (NoS)	ResNet-50	D -> W	(0.001-0.0001)	0.001	0.001	32,64	224X224	min(TVL)	5000
PIXELDA	ResNet-50	D -> W	(0.001-0.0001)	0.0005	N/A	32,64	224X224	min(TVL)	N/A
GAGL	ResNet-50	W -> A	(0.001-0.0001)	0.001	0.0005	32,64	224X224	min(TVL)	5000
MD-nets	ResNet-50	W -> A	(0.001-0.0001)	0.001	0.0005	32,64	224X224	min(SVL)	5000
MD-nets (NoS)	ResNet-50	W -> A	(0.001-0.0001)	0.0001	0.001	32,64	224X224	min(TVL)	5000
PIXELDA	ResNet-50	W -> A	(0.001-0.0001)	0.0005	N/A	32,64	224X224	min(TVL)	N/A
GAGL	ResNet-50	W -> D	(0.001-0.0001)	0.001	0.0005	32,64	224X224	min(TVL)	5000
MD-nets	ResNet-50	W -> D	(0.001-0.0001)	0.001	0.0005	32,64	224X224	min(SVL)	5000
MD-nets (NoS)	ResNet-50	W -> D	(0.001-0.0001)	0.0001	0.001	32,64	224X224	min(TVL)	5000
PIXELDA	ResNet-50	W -> D	(0.001-0.0001)	0.0001	N/A	32,64	224X224	min(TVL)	N/A
ADDA	ResNet-50	EM4	(0.01-0.0001)	0.01	0.0005	32,64	224X224	min(TVL)	5000
CAN	ResNet-50	EM4	(0.01-0.0001)	0.01	0.0005	32,64	224X224	DC <0.0001	N/A
DANN	ResNet-50	EM4	(0.01-0.0001)	0.01	0.0005	32,64	224X224	min(SVL)	5000

GAGL	ResNet-50	EM4	(0.01-0.0001)	0.01	0.0005	32,64	224X224	min(TVL)	5000
MD-nets	Xception	EM4	(0.1-0.0001)	0.01	0.0005	32,64	224X224	min(SVL)	2000
MD-nets	ResNet-50	EM4	(0.01-0.0001)	0.01	0.0005	32,64	224X224	min(SVL)	2000
PIXELD A	ResNet-50	EM4	(0.01-0.0001)	0.01	0.0005	16,32,64	224X224	min(TVL)	N/A
ADDA	ResNet-50	EM41	(0.01-0.0001)	0.01	0.0005	32,64	224X224	min(TVL)	5000
CAN	ResNet-50	EM41	(0.01-0.0001)	0.01	0.0005	32,64	224X224	DC <0.0001	N/A
DANN	ResNet-50	EM41	(0.01-0.0001)	0.01	0.0005	32,64	224X224	min(SVL)	5000
GAGL	ResNet-50	EM41	(0.01-0.0001)	0.01	0.0005	32,64	224X224	min(TVL)	5000
MD-nets	Xception	EM41	(0.1-0.0001)	0.01	0.0005	32,64	224X224	min(SVL)	2000
MD-nets	ResNet-50	EM41	(0.01-0.0001)	0.01	0.0005	32,64	224X224	min(SVL)	2000
PIXELD A	ResNet-50	EM41	(0.01-0.0001)	0.01	0.0005	16,32,64	224X224	min(TVL)	N/A
ADDA	ResNet-50	EM42	(0.01-0.0001)	0.01	0.0005	32,64	224X224	min(TVL)	5000
CAN	ResNet-50	EM42	(0.01-0.0001)	0.01	0.0005	32,64	224X224	DC <0.0001	N/A
DANN	ResNet-50	EM42	(0.01-0.0001)	0.01	0.0005	32,64	224X224	min(SVL)	5000
GAGL	ResNet-50	EM42	(0.01-0.0001)	0.01	0.0005	32,64	224X224	min(TVL)	5000
MD-nets	Xception	EM42	(0.1-0.0001)	0.01	0.0005	32,64	224X224	min(SVL)	2000
MD-nets	ResNet-50	EM42	(0.01-0.0001)	0.01	0.0005	32,64	224X224	min(SVL)	2000
PIXELD A	ResNet-50	EM42	(0.01-0.0001)	0.01	0.0005	16,32,64	224X224	min(TVL)	N/A
ADDA	ResNet-50	EM43	(0.01-0.0001)	0.01	0.0005	32,64	224X224	min(TVL)	5000
CAN	ResNet-50	EM43	(0.01-0.0001)	0.01	0.0005	32,64	224X224	DC <0.0001	N/A
DANN	ResNet-50	EM43	(0.01-0.0001)	0.01	0.0005	32,64	224X224	min(SVL)	5000
GAGL	ResNet-50	EM43	(0.01-0.0001)	0.01	0.0005	32,64	224X224	min(TVL)	5000
MD-nets	Xception	EM43	(0.1-0.0001)	0.01	0.0005	32,64	224X224	min(SVL)	2000
MD-nets	ResNet-50	EM43	(0.01-0.0001)	0.01	0.0005	32,64	224X224	min(SVL)	2000
PIXELD A	ResNet-50	EM43	(0.01-0.0001)	0.01	0.0005	16,32,64	224X224	min(TVL)	N/A
MD-nets (NoS)	ResNet-50	MM(nos) 1 t	(0.01-0.0001)	0.0005	0.0005	8,16,32	100X100	min(TVL)	5000
MD-nets (NoS)	ResNet-50	MM(nos) 2	(0.01-0.0001)	0.003	0.0005	8,16,32	100X100	min(TVL)	5000
MD-nets (NoS)	ResNet-50	MM(nos) 3	(0.01-0.0001)	0.01	0.0005	8,16,32	100X100	min(TVL)	5000
MD-nets	ResNet-50	MM1_s1 t	(0.001-0.0001)	0.001	0.0005	16,32	100X100	min(SVL)	2000
MD-nets	ResNet-50	MM1_s2	(0.001-0.0001)	0.0001	0.0005	16,32	100X100	min(SVL)	2000
MD-nets	ResNet-50	MM1_s3	(0.001-0.0001)	0.0001	0.0005	16,32	100X100	min(SVL)	2000
MD-nets (SW)	ResNet-50	MM1_s1 t	(0.001-0.0001)	0.01	0.0005	16,32	100X100	min(SVL)	5000
MD-nets (SW)	ResNet-50	MM1_s2	(0.001-0.0001)	0.003	0.0005	16,32	100X100	min(SVL)	5000
MD-nets (SW)	ResNet-50	MM1_s3	(0.001-0.00001)	0.00001	0.0005	16,32	100X100	min(SVL)	5000
MD-nets	Xception	SM4	(0.01-0.00001)	0.01	0.0005	16,32,64	224X224	min(SVL)	2000
MD-nets	Xception	SM41	(0.01-0.0001)	0.001	0.0005	8,16,32	130X130	min(SVL)	2000
MD-nets	Xception	SM42	(0.01-0.00001)	0.001	0.0005	16,32,64	280X280	min(SVL)	2000
MD-nets	Xception	SM43	(0.01-0.00001)	0.01	0.0005	16,32,64	224X224	min(SVL)	2000